

See discussions, stats, and author profiles for this publication at: <https://www.researchgate.net/publication/26735024>

Synthesis, Biological Evaluation, and Three-Dimensional in Silico Pharmacophore Model for σ 1 Receptor Ligands Based on a Series of Substituted Benzo[d]oxazol-2(3 H)-one Derivat...

ARTICLE in JOURNAL OF MEDICINAL CHEMISTRY · SEPTEMBER 2009

Impact Factor: 5.45 · DOI: 10.1021/jm900366z · Source: PubMed

CITATIONS

40

READS

78

10 AUTHORS, INCLUDING:



Maria Grazia Mamolo

Università degli Studi di Trieste

54 PUBLICATIONS 750 CITATIONS

SEE PROFILE



Chiara Florio

Università degli Studi di Trieste

63 PUBLICATIONS 955 CITATIONS

SEE PROFILE



Maurizio Fermeglia

Università degli Studi di Trieste

221 PUBLICATIONS 3,191 CITATIONS

SEE PROFILE



Sabrina Prici

Università degli Studi di Trieste

247 PUBLICATIONS 3,769 CITATIONS

SEE PROFILE

Synthesis, Biological Evaluation, and Three-Dimensional in Silico Pharmacophore Model for σ_1 Receptor Ligands Based on a Series of Substituted Benzo[d]oxazol-2(3H)-one Derivatives

Daniele Zampieri,[‡] Maria Grazia Mamolo,^{*,‡} Erik Laurini,[‡] Chiara Florio,[†] Caterina Zanette,[†] Maurizio Fermeglia,[§] Paola Posocco,[§] Maria Silvia Paneni,[§] Sabrina Pricl,^{*,§} and Luciano Vio[‡]

[‡]Department of Pharmaceutical Sciences, Piazzale Europa 1, University of Trieste, 34127 Trieste, Italy, [†]Department of Life Sciences, Section of Pharmacology, University of Trieste, 34127 Trieste, Italy, and [§]Department of Chemical, Environmental, and Raw Materials Engineering (DICAMP), Molecular Simulation Engineering (MOSE) Laboratory, Piazzale Europa 1, University of Trieste, 34127 Trieste, Italy

Received March 23, 2009

Novel benzo[d]oxazol-2(3H)-one derivatives were designed and synthesized, and their affinities against σ receptors were evaluated. On the basis of 31 compounds, a three-dimensional pharmacophore model for the σ_1 receptor binding site was developed using the Catalyst 4.9 software package. The best 3D pharmacophore hypothesis, consisting of one positive ionizable, one hydrogen bond acceptor, two hydrophobic aromatic, and one hydrophobic features provided a 3D-QSAR model with a correlation coefficient of 0.89. The best hypothesis was also validated by three independent methods, i.e., the Fisher randomization test included in the CatScramble functionality of Catalyst, the leave-one-out test, and activity prediction of an additional test set. The achieved results will allow researchers to use this 3D pharmacophore model for the design and synthesis of a second generation of high affinity σ_1 ligands, as well as to discover other lead compounds for this class of receptors.

Introduction

The σ binding sites were originally defined and classified as opioid receptor subtypes.¹ Later investigations demonstrated that σ receptors were distinct from opioid and phencyclidine analogues, and since then, at least two distinct σ receptor subtypes, designated σ_1 and σ_2 ,² have been pharmacologically characterized.^{3–5} The cellular and anatomical distribution of σ receptors is not restricted to the central nervous system (CNS),^{6–8} but extends to peripheral tissues such as blood vessels, adrenal glands, testicles, ovaries, and immune system.⁹ There is increasing evidence that σ receptors have a neuromodulatory role in the CNS and are involved in the etiology of various psychiatric diseases¹⁰ such as anxiety, schizophrenia, and depression. The correlation between the extent of toxic effects on CNS of some antipsychotic compounds and their σ receptor affinity is also documented. Furthermore, σ receptors may also have a potential role

in neuromotor diseases such as dystonia and dyskinesia;¹¹ indeed, σ receptors are highly expressed in brain areas associated with the control of movement of facial muscles.¹¹

The σ_1 receptor subtype has been purified and cloned from several animal species and man.^{12,13} Its primary sequence is now available and shows remarkable homology with sterol C8–C7 isomerase from fungi. The σ_1 receptors exert a modulatory role on neurotransmitter systems such as dopaminergic, serotonergic, and muscarinic systems^{5,14,15} and on the NMDA-stimulated neurotransmitters' release.¹⁶ Moreover, σ_1 receptors are involved in neuroprotective and anti-amnesic activities,¹⁷ modulation of opioid analgesia,¹⁸ and attenuation of cocaine-induced locomotor activity and toxicity.¹⁹ In addition, σ_1 antagonists have been shown to be effective against negative symptoms of schizophrenia without producing extrapyramidal side effects typical of traditional neuroleptics.^{20,21}

On the other hand, the molecular identity of the σ_2 receptor subtype has not been fully determined,^{12,13} although a number of studies have presented evidence linking σ_2 receptors to potassium channels and intracellular calcium release in NCB-20 cells.^{22,23} Unlike the σ_1 subtype, σ_2 receptors may contribute to the acute side effects of typical neuroleptic drugs, and σ_2 antagonists are known to attenuate extrapyramidal effects, dystonic reactions, and tardive dyskinesia,^{2,14,22,24,25} suggesting their potential use in the treatment of psychoses.^{20,21} Furthermore, σ_2 receptors are involved in the regulation of cell proliferation and maintenance of cell viability. They are highly expressed in several tumoral cell lines,^{26,27} where σ_2 agonists produce morphological changes and apoptosis. The σ_2 receptor agonists promote Ca^{2+} release from endoplasmic reticulum and mitochondrial stores,²⁸ with subsequent cell death by

*To whom correspondence should be addressed. For M.G.M. (chemistry and biological sections): phone, +390405583719; fax, +39040525272; e-mail, mamolo@units.it. For S.P. (computational and molecular modeling sections): phone, +390405583750; fax, +39040569823; e-mail, sabrina.pricl@dicamp.units.it.

^a Abbreviations: 3D-QSAR, three-dimensional quantitative structure–activity relationship; CNS, central nervous system; NMDA, N-methyl D-aspartate; NCB-20, mouse neuroblastoma Chinese hamster brain hybrid cell line; PET, positron-emission tomography; SPECT, single photon emission computed tomography; PTZ, (+)-pentazocine; NANM, (+)-N-allylnormetazocine; DMAP, 4-dimethylaminopyridine; TFA, trifluoroacetic acid; PC, positive charge; NC, negative charge; HBD, hydrogen bond donor; HBA, hydrogen bond acceptor; HBAI, hydrogen bond acceptor lipid; HYAr, hydrophobic aromatic; HY, generic hydrophobic; Ar, ring aromatic; PI, positive ionizable; rmsd, root-mean-square deviation; ERG2, ether-a-go-go related gene 2; SEM, standard error of the mean.

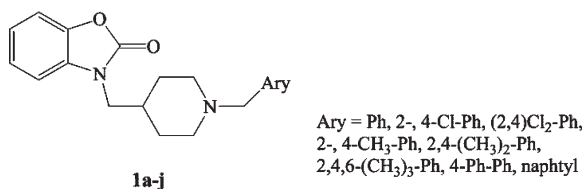


Figure 1. Structures of compounds **1a–j**.

caspase-independent apoptosis.²⁷ Apoptosis may also be induced in tumoral cells by regulation of the sphingolipid pathway.²⁹ Therefore, σ_2 agonists may be useful as novel anticancer agents and as imaging agents in cancer diagnosis by positron emission tomography (PET)³⁰ and single photon emission computed tomography (SPECT).^{31,32}

To date, well-known compounds characterized by a certain degree of selectivity for the σ_1 receptor subtype include (+)-benzomorphans such as (+)-pentazocine (PTZ) and (+)-N-allylnormetazocine (NANM, SKF-10047), while haloperidol and 1,3-di-(2-tolyl)guanidine show high affinity for both receptor subtypes.²²

In our previous work³³ we described the synthesis and the affinities for the σ receptors of a series of substituted benzoxazolone derivatives **1a–j** (Figure 1), in which the benzyl group was variously substituted at the phenyl ring. The benzoxazolone derivatives **1a–j** have been designed according to the σ_1 receptor model proposed by Glennon,^{34–36} under the following assumptions: (i) the benzoxazolone moiety may interact with a primary hydrophobic site corresponding to Glennon's phenyl "B" region;^{34–36} (ii) the 4-methylpiperidin-1-yl spacer links the basic nitrogen atom to the benzoxazolone moiety; (iii) the substituted *N*-benzyl moiety may bind the secondary hydrophobic phenyl "A" region of the σ_1 receptor model, modulating the binding affinity of the compounds for the σ receptors.

The relevant results indicated that the substituents on the phenyl ring can modulate the σ_1 and σ_2 binding affinities of these compounds. Indeed, all molecules show, to various degrees, a preference for σ_1 receptor sites, with the unsubstituted derivative and the corresponding para-substituted derivatives exhibiting the highest affinity. Particularly, the best result was reached with the 4-chloro substituted compound, with a $K_i(\sigma_1)$ value of 0.1 nM and a $K_i(\sigma_2)/K_i(\sigma_1)$ selectivity ratio of 4270.

In this work we synthesized (Scheme 1) a series of 3-[(*N*-benzyl-*N*-ethylamine)alkyl]benzo[d]oxazol-2(3*H*)-one derivatives **2a–k** and **3a–k** (Table 1), with various substitutions at the benzene ring, to generate an adequate number of compounds for the purpose of developing a three-dimensional (3D) pharmacophore model for σ_1 receptor ligands.

Since the benzoxazolone moiety is considered to form a good interaction with a putative hydrophobic region in these receptors, this group has been maintained in the new molecular series. Moreover, the electronegative atoms of the oxazolone moiety may further contribute to the binding affinity. Effectively, electronegative atoms such as O or S are frequently present in very potent σ_1 ligands, bridging the aromatic component and the classical alkyl or cycloalkyl intermediate spacer linked to the basic nitrogen atom.^{13,36} On the basis of a molecular modeling study of σ_1 receptor ligands, Gund et al.³⁷ also concluded that there could be a secondary binding region that may surround the oxygen or sulfur atom of the molecules. In the other half of the molecule, the piperidin-4-ylmethyl core has been replaced by an alkyl

Scheme 1. Synthesis of Compounds **2a–k** and **3a–k**

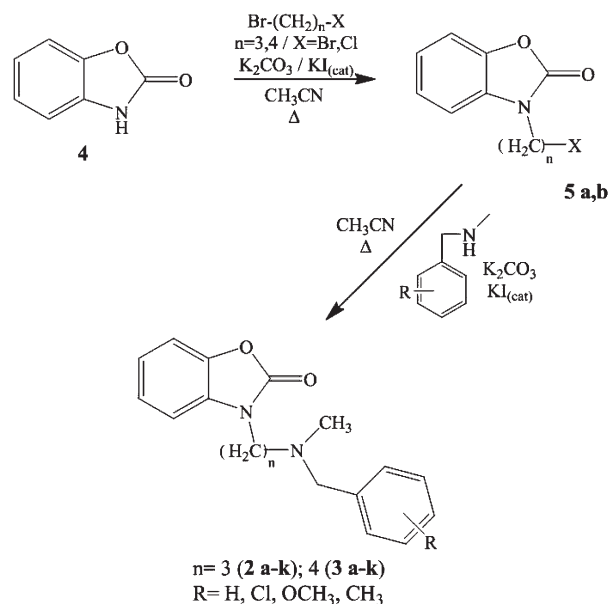


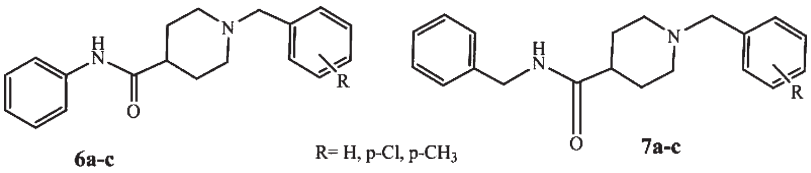
Table 1. Physical and Chemical Data for Compounds **2a–k** and **3a–k**

n=3 (2 a-k); 4 (3 a-k)
R= H, Cl, OCH₃, CH₃

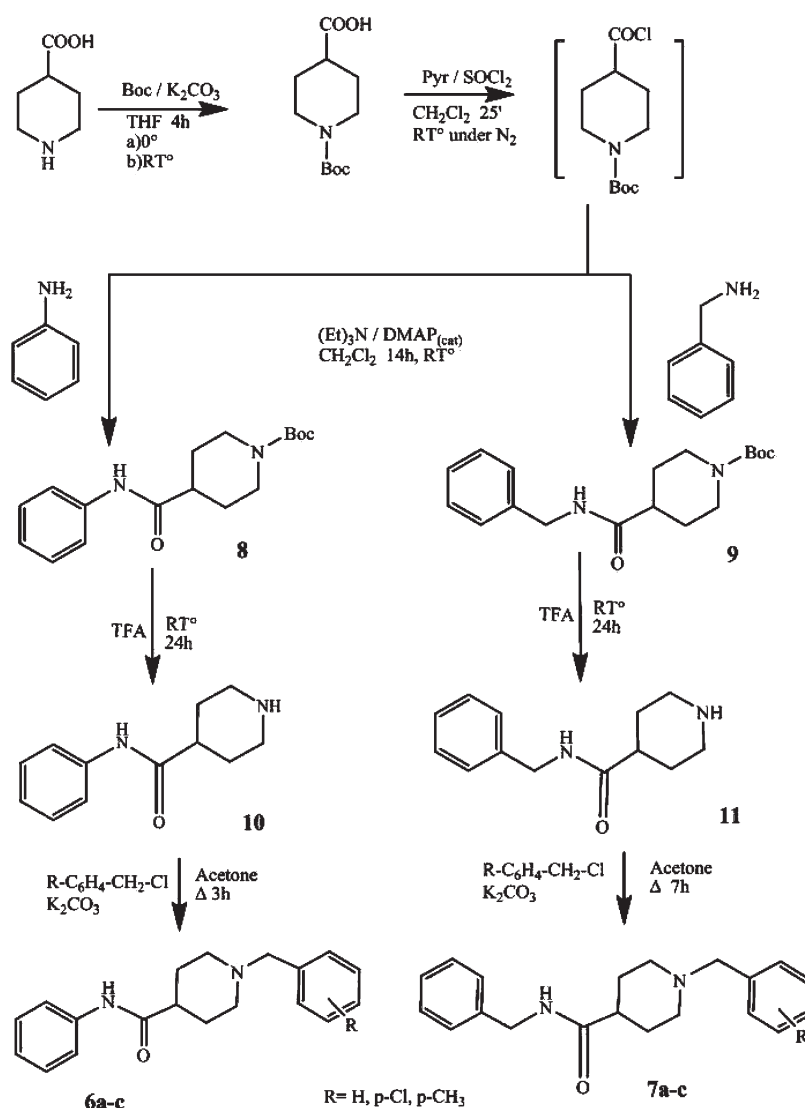
compd	R	n	mp (°C) ^a	yield (%)	formula	Anal. ^b
2a	H	3	180–182	30	C ₂₀ H ₂₂ N ₂ O ₆	C, H, N
2b	2-Cl	3	129–131	33	C ₂₀ H ₂₁ ClN ₂ O ₆	C, H, N
2c	3-Cl	3	166–168	27	C ₂₀ H ₂₁ ClN ₂ O ₆	C, H, N
2d	4-Cl	3	192–194	30	C ₂₀ H ₂₁ ClN ₂ O ₆	C, H, N
2e	2-OCH ₃	3	145–147	15	C ₂₁ H ₂₄ N ₂ O ₇	C, H, N
2f	3-OCH ₃	3	168–170	18	C ₂₁ H ₂₄ N ₂ O ₇	C, H, N
2g	4-OCH ₃	3	179–183	21	C ₂₁ H ₂₄ N ₂ O ₇	C, H, N
2h	2-CH ₃	3	167–169	10	C ₂₁ H ₂₄ N ₂ O ₆	C, H, N
2i	3-CH ₃	3	156–158	39	C ₂₁ H ₂₄ N ₂ O ₆	C, H, N
2j	4-CH ₃	3	195–197	41	C ₂₁ H ₂₄ N ₂ O ₆	C, H, N
2k	2,4-(CH ₃) ₂	3	127–130	53	C ₂₂ H ₂₆ N ₂ O ₆	C, H, N
3a	H	4	145–147	30	C ₂₁ H ₂₄ N ₂ O ₆	C, H, N
3b	2-Cl	4	115–117	23	C ₂₁ H ₂₃ ClN ₂ O ₆	C, H, N
3c	3-Cl	4	168–170	23	C ₂₁ H ₂₃ ClN ₂ O ₆	C, H, N
3d	4-Cl	4	162–164	46	C ₂₁ H ₂₃ ClN ₂ O ₆	C, H, N
3e	2-OCH ₃	4	127–129	15	C ₂₂ H ₂₆ N ₂ O ₇	C, H, N
3f	3-OCH ₃	4	154–156	19	C ₂₂ H ₂₆ N ₂ O ₇	C, H, N
3g	4-OCH ₃	4	98–100	55	C ₂₂ H ₂₆ N ₂ O ₇	C, H, N
3h	2-CH ₃	4	212–214	11	C ₂₂ H ₂₆ N ₂ O ₆	C, H, N
3i	3-CH ₃	4	169–171	49	C ₂₂ H ₂₆ N ₂ O ₆	C, H, N
3j	4-CH ₃	4	138–140	42	C ₂₂ H ₂₆ N ₂ O ₆	C, H, N
3k	2,4-(CH ₃) ₂	4	103–105	40	C ₂₃ H ₂₈ N ₂ O ₆	C, H, N

^aThe melting points refer to the compounds as oxalate salts. ^bAll compounds were analyzed to be within $\pm 0.3\%$ of the theoretical values.

spacer, endowed with greater conformational freedom. The choice of a propyl or butyl chain is dictated by the fact that both fall within the range of optimal distances between the basic nitrogen atom and hydrophobic primary site in the receptor

Table 2. Physical and Chemical Data for Compounds **6a–c** and **7a–c**


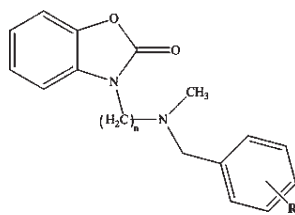
compd	R	mp (°C)	yield (%)	formula	Anal. ^a
6a	H	138–140	66	C ₁₉ H ₂₂ N ₂ O	C, H, N
6b	4-Cl	188–190	70	C ₁₉ H ₂₁ ClN ₂ O	C, H, N
6c	4-CH ₃	162–164	63	C ₂₀ H ₂₄ N ₂ O	C, H, N
7a	H	110–112	75	C ₂₀ H ₂₄ N ₂ O	C, H, N
7b	4-Cl	137–141	72	C ₂₀ H ₂₃ ClN ₂ O	C, H, N
7c	4-CH ₃	112–114	68	C ₂₁ H ₂₆ N ₂ O	C, H, N

^a All compounds were analyzed to be within $\pm 0.3\%$ of the theoretical values.**Scheme 2.** Synthesis of Compounds **6a–c** and **7a–c**

model of Glennon.^{34–36} All compounds obtained were subsequently tested in order to assess their affinity and their selectivity toward σ receptors.

As mentioned previously, the crystal structure of both σ_1 and σ_2 receptors remains unsolved to date. In the absence of a reliable 3D model of the target structure, ligand-based

molecular modeling tools can be successfully employed to devise structural requirements crucial for receptor binding. The 3D quantitative structure–activity relationship (3D-QSAR) pharmacophore modeling is such an approach and constitutes a consolidated technique in drug design and discovery.

Table 3. Binding Affinities of Compounds **2a–k**, **3a–k**, [³H]-(+)-Pentazocine (σ_1), and [³H]-DTG (σ_2) Binding Sites in Rat Liver Homogenate^an = 3 (**2a–k**), 4 (**3a–k**)

compd	n	R	$K_i(\sigma_1)$ (nM) ^b	n_H ^b	$K_i(\sigma_2)$ (nM) ^b	n_H ^b	σ_2/σ_1 ratio
2a	3	H	223 ± 47	1.12 ± 0.23	1121 ± 603	0.80 ± 0.21	5.0
2b	3	2-Cl	2492 ± 115	1.13 ± 0.07	456 ± 154	0.92 ± 0.28	0.18
2c	3	3-Cl	3233 ± 447	1.67 ± 0.34	1119 ± 722	0.60 ± 0.28	0.35
2d	3	4-Cl	1147 ± 206	1.09 ± 0.19	456 ± 154	0.66 ± 0.39	0.40
2e	3	2-OCH ₃	1947 ± 136	1.57 ± 0.14	192 ± 130	2.04 ± 0.51	0.10
2f	3	3-OCH ₃	8550 ± 500	1.75 ± 0.16	2130 ± 295	0.95 ± 0.07	0.16
2g	3	4-OCH ₃	83 ± 17	0.95 ± 0.17	2602 ± 714	0.96 ± 0.13	31.3
2h	3	2-CH ₃	901 ± 107	0.99 ± 0.10	1347 ± 99	1.16 ± 0.29	1.5
2i	3	3-CH ₃	1835 ± 159	1.71 ± 0.22	2716 ± 1847	1.03 ± 0.39	1.5
2j	3	4-CH ₃	871 ± 159	1.06 ± 0.18	991 ± 180	1.17 ± 0.20	1.1
2k	3	2,4-(CH ₃) ₂	1833 ± 204	1.87 ± 0.29	2064 ± 11	2.41 ± 0.03	1.1
3a	4	H	2.6 ± 1.5	0.45 ± 0.09	120 ± 40	0.80 ± 0.23	46.2
3b	4	2-Cl	843 ± 217	1.62 ± 0.58	37.4 ± 16	0.55 ± 0.14	0.04
3c	4	3-Cl	302 ± 112	0.87 ± 0.32	ND ^c		ND ^c
3d	4	4-Cl	7.1 ± 1.5	0.72 ± 0.10	36.2 ± 6.5	1.12 ± 0.20	5.1
3e	4	2-OCH ₃	594 ± 96	0.87 ± 0.13	ND ^c		ND ^c
3f	4	3-OCH ₃	297 ± 34	1.69 ± 0.32	187 ± 13	1.57 ± 0.15	0.6
3g	4	4-OCH ₃	21 ± 3.8	0.76 ± 0.11	20.8 ± 4.3	1.11 ± 0.23	1
3i	4	3-CH ₃	102 ± 7.4	0.40 ± 0.13	31.8 ± 5.3	0.96 ± 0.14	0.31
3j	4	4-CH ₃	97 ± 7.3	1.03 ± 0.07	22.9 ± 2.8	1.08 ± 0.13	0.20
3k	4	2,4-(CH ₃) ₂	239 ± 27	0.95 ± 0.09	6.94 ± 5.2	0.34 ± 0.09	0.03
(+)-pentazocine			15 ± 3	0.88 ± 0.14	327 ± 166	0.88 ± 0.25	22
DTG			180 ± 22	1.30 ± 0.20	130 ± 46	1.50 ± 0.67	0.72
haloperidol (12)			5.7 ± 1	0.55 ± 0.07	235 ± 71	0.85 ± 0.19	41

^a n_H = Hill coefficient. ^b Standard error of the mean. ^c ND: not determined.

The major goal this paper is the generation of a predictive pharmacophore model for σ_1 ligands. To develop the model, we resorted to the HypoGen method implemented in the Catalyst software package.³⁸ Starting with a training set of 31 σ_1 ligands, a pharmacophore model (also called a hypothesis) able to quantitatively correlate the estimated affinities with the corresponding measured values was generated. The model was then validated by statistical means and by its ability to predict the affinity of a further ensemble of different compounds (test set). Overall, we verified that our 3D-QSAR pharmacophore model was predictive not only within the training set but also for the test set compounds, with acceptable errors.

Chemistry

The substituted 3-[3-(*N*-benzyl-*N*-methylamino)propyl]benzo[d]oxazol-2(3*H*)-one derivatives **2a–k** and 3-[4-(*N*-benzyl-*N*-methylamino)butyl]benzo[d]oxazol-2(3*H*)-one derivatives **3a–k** were synthesized (Scheme 1) by treating an acetonitrile solution of benzo[d]oxazol-2(3*H*)-one **4** with 1-bromo-3-chloropropane and 1,4-dibromobutane, respectively, in the presence of K₂CO₃ and a catalytic amount of KI. From the obtained 3-(3-chloropropyl) and 4-(4-bromobutyl)benzo[d]oxazol-2(3*H*)-one intermediates **5a,b**, the substituted *N*-benzyl derivatives were obtained by heating at reflux with *N*-methylbenzylamines in acetonitrile in the presence of K₂CO₃ and a catalytic amount of KI.

The substituted 1-benzyl-*N*-phenylpiperidine-4-carboxamide derivatives **6a–c** and the corresponding *N*-benzyl derivatives **7a–c** were prepared starting from the commercially available 4-piperidinecarboxylic acid which was transformed into the corresponding *N*-boc-4-piperidinecarboxylic chloride by treatment with SOCl₂ under N₂ (Table 2 and Scheme 2). A solution of aniline and triethylamine in CH₂Cl₂ was added directly to the reaction mixture with a catalytic amount of DMAP. The reaction was carried out at room temperature under N₂ flux to afford *N*-phenyl-1-(*tert*-butoxycarbonyl)piperidine-4-carboxamide **8**, which was deprotected with TFA to yield the *N*-phenylpiperidine-4-carboxamide **10**.

Following the same route described above and using benzylamine, *N*-benzyl-1-(*tert*-butoxycarbonyl)piperidine-4-carboxamide **9** was prepared, from which *N*-benzylpiperidine-4-carboxamide **11** was obtained after deprotection with TFA. From the piperidine-4-carboxamides **10** and **11**, the corresponding 1-benzyl derivatives **6a–c** and **7a–c** were obtained by alkylation with the opportune benzyl chlorides.

Results and Discussion

On the basis of the interesting $K_i(\sigma_1)$ values of a series of benzo[d]oxazolone derivatives **1a–j** (Figure 1) we described in previous work,³³ we synthesized a series of new benzoxazolone derivatives **2a–k** and **3a–k** (Table 1) in which the 4-methylpiperidin-1-yl spacer linking the benzoxazolone moiety to the benzyl group was replaced by the 3-(*N*-methylamino)propyl

Table 4. Experimental and Estimated Affinity Values of the Training Test Compounds

compd	R	$K_i(\sigma_1)$ (nM)		error ^a
		experimental	estimated	
1a	H	3.58	18	5.0
1b	2-Cl	60.9	60	-1.0
1c	4-Cl	0.098	0.27	2.8
1d	2,4-Cl	258	280	1.1
1e	2-CH ₃	29.8	160	5.4
1f	4-CH ₃	3.07	1	-3.1
1g	2,4-CH ₃	30.2	210	7.0
1h	2,4,6-CH ₃	6210	660	-9.4
1i	4-Ph	394	230	-1.7
1j	naphthyl	1017	670	-1.5
2a	H	223	550	2.5
2b	2-Cl	2492	6700	2.7
2c	3-Cl	3233	1110	-2.9
2d	4-Cl	1147	960	-1.2
2e	2-OCH ₃	1947	3600	1.8
2f	3-OCH ₃	8550	880	-9.7
2g	4-OCH ₃	83	56	-1.5
2h	2-CH ₃	901	2000	2.2
2i	3-CH ₃	1835	4000	2.2
2j	4-CH ₃	871	410	-2.1
2k	2,4-(CH ₃) ₂	1833	1400	-1.3
3a	H	2.6	24	9.2
3b	2-Cl	843	140	-6.0
3c	3-Cl	302	450	1.5
3d	4-Cl	7.1	16	2.3
3e	2-OCH ₃	594	260	-2.3
3f	3-OCH ₃	297	140	-2.1
3g	4-OCH ₃	21	42	2.0
3i	3-CH ₃	102	100	-1.0
3j	4-CH ₃	97	270	2.8
3k	2,4-(CH ₃) ₂	239	860	3.6

^a Values in the error column represent the ratio of the estimated to experimental affinity, or its negative inverse if the ratio is less than 1.

and 4-(*N*-methylamino)butyl groups, respectively. The aim was to verify if these modifications might produce compounds retaining affinity for σ receptor sites. All compounds were tested to evaluate their K_i values against both σ_1 and σ_2 subtypes (Table 3).

From the results obtained so far (Table 3), it appears that the substituents on the phenyl ring strongly modulate the σ_1 and σ_2 binding affinity of these compounds, butylene derivatives **3a–k** having higher affinity than the corresponding propylene derivatives **2a–k**, as in the case of compounds **1a–j**.³³ The butylene intermediate chain determines the optimal distance between the primary B and secondary A hydrophobic centers proposed by the Glennon's model.^{34–36} The compound with the highest affinity is the butylene derivative **3a** (R = H), with $K_i(\sigma_1)$ value of 2.6 nM and an interesting selectivity ratio $K_i(\sigma_2)/K_i(\sigma_1) = 46.2$. The para-substituted compound **3d** (R = 4-Cl), instead, still maintains an appreciable σ_1 affinity but has a selectivity ratio ($K_i(\sigma_2)/K_i(\sigma_1) = 5.1$) lower than those of the unsubstituted derivatives.

Unlike the derivatives previously described, compound **3g** (R = 4-OCH₃) has no selectivity, showing a moderate affinity toward both receptors. On the other hand, compounds **3b** and **3i–k** show preference toward the σ_2 receptor. Specifically, compound **3k** (R = 2,4-(CH₃)₂) has the highest σ_2 affinity ($K_i(\sigma_2) = 6.94$ nM) and selectivity ratio ($K_i(\sigma_2)/K_i(\sigma_1) = 0.03$) of the series.

For the development of a 3D quantitative structure–activity relationship (3D-QSAR) pharmacophore model,

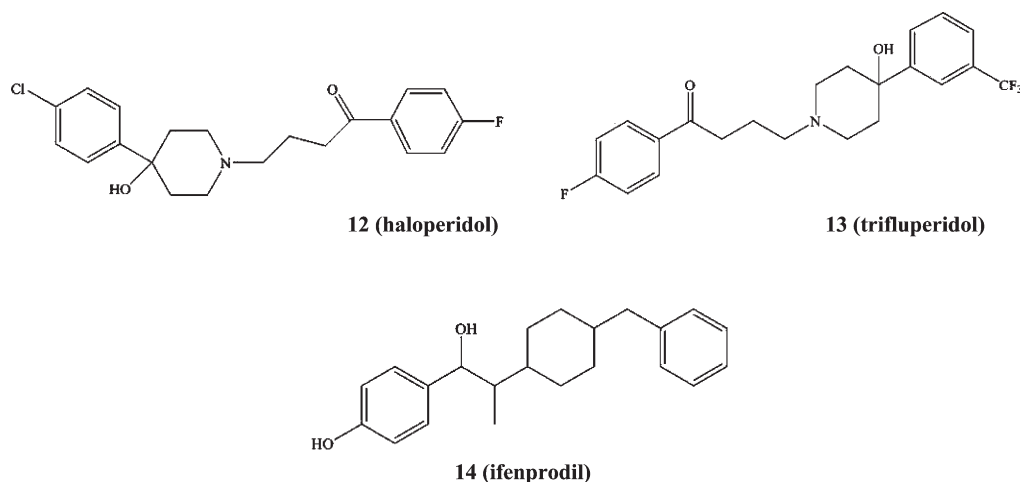
a training set was derived with 31 compounds from our series, considering structural diversity and the widest possible coverage of the in vitro affinity range (see Table 4). To validate the developed pharmacophore model, we then predicted the σ_1 affinity of the test set of piperidine-4-carboxamide derivatives **6a–c** and **7a–c** and the reference σ_1 ligands haloperidol **12**, trifluoperidol **13**, and ifenprodil **14**. Compounds **6a–c** and **7a–c** were synthesized (Scheme 2), their $K_i(\sigma_1)$ values were determined, and their estimated σ_1 affinities were compared with the experimental data (Table 5).

3D Pharmacophore Modeling. In this work we developed a three-dimensional pharmacophore model in order to have a tool to design a second generation of σ_1 receptor ligands. It is a widely accepted that 3D pharmacophore modeling is a well-behaved approach to quantitatively explore the common chemical characteristics among a considerable number of different structures. However, a computed pharmacophore model can only be as good as the information that it contains. To achieve a quality model, at least three must-obey rules should be respected in three-dimensional quantitative structure–activity relationship (3D-QSAR) generation: (i) the training set must include a wide population (at least 16 items) of diverse compounds covering at least 4 orders of magnitude of activity; (ii) the most active compound should be included in the training set; (iii) all biological data must be obtained by homogeneous procedures.^{39,40}

In our case, a training set consisting of 31 compounds from our series was prepared by considering structural diversity and the widest possible coverage of the in vitro affinity range (see Table 4). The molecules in our training set were selected according to the following criteria: (i) the training set should contain structures from each series of active compounds; (ii) the training set should cover the molecular bioactivities (K_i) as widely as possible. Should there be only one compound with maximum or minimum order of bioactivity in a series, then this compound was assigned to the training set.

The HypoGen algorithm allows a maximum of five features to be considered in the pharmacophore generation process. Accordingly, from the 11 features available in the Catalyst features dictionary (see Experimental Section for details), we excluded all those that clearly did not match the chemistry of the molecules of the training set, such as positive charge (PC) and negative charge (NC), as all ligands were considered in their neutral form. Also, preliminary runs including the hydrogen bond donor (HBD) and hydrogen bond acceptor lipid (HBAI) features confirmed that these features were never used in the generation of the pharmacophore models, even though they were present and properly mapped on several molecules of the training set. Thus, the HBD and HBAI features were removed from the list. Moreover, as most of the molecules in the training set possess both hydrophobic aromatic and hydrophobic aliphatic groups, the specific hydrophobic aromatic (HYAr) and hydrophobic aliphatic (HYAl) features were both selected. The more generic hydrophobic feature (HY) was also chosen to optimize the substituents mapping on the phenyl ring. In summary, the following five chemical features were taken into account for hypothesis generation with HypoGen: hydrogen bond acceptor (HBA), hydrophobic aromatic (HYAr), hydrophobic aliphatic (HYAl), ring aromatic (Ar), and positive ionizable (PI).

In total, 10 hypotheses were generated by the HypoGen algorithm, all characterized by 5 features. The total

Table 5. Experimental and Estimated Affinity Values of the Test Set Compounds

compd	R	$K_i(\sigma_1)$ (nM)		error ^a
		experimental	estimated	
6a	H	48.1	210	4.4
6b	4-Cl	45.0	140	3.1
6c	4-CH ₃	105	200	1.9
7a	H	22.5	37	1.6
7b	4-Cl	12.9	5.5	-2.3
7c	4-CH ₃	69.4	76	1.1
12		5.7	2.2	-2.6
13		0.8	4.6	5.8
14		2.0	19	9.5

^a Values in the error column represent the ratio of the estimated to experimental affinity, or its negative inverse if the ratio is less than 1.

hypothesis cost of these 10 best models varies between 124.1 for the best ranked model (Hypo1) to 151.2 for the lowest ranked one (Hypo10). Such a confined difference (27 bits) reflects both the homogeneity of the generated hypotheses and the adequacy of the molecular training set. The difference between the null and the fixed costs, which should be higher than 70 to guarantee a robust correlation, is 91 in our case. This corresponds to a chance of true correlation in the data greater than 90%.⁴¹ Furthermore, in all the generated hypotheses the total costs are much closer to the fixed cost (103.1) than to the null cost (194.1), indicating that meaningful models are obtained. Finally, the root-mean-square deviations (rmsd) and the correlation coefficients (ρ) between estimated and experimental affinities range from 1.126 to 1.844 and from 0.896 to 0.566, respectively. As all the generated pharmacophores map the molecules of the training set in a similar way, the first model (Hypo1), characterized by the highest cost difference, the lowest rmsd, and the best ρ values, was selected for further analysis.

Hypo1 contains one hydrogen bond acceptor, two hydrophobic aromatic features, one hydrophobic feature, and one positive ionizable group. The affinities of the 31 compounds estimated using Hypo1 are reported in Table 4, along with the experimental values and the relevant errors (expressed as the ratio of estimated to experimental values). This table clearly shows that 24 out of 31 molecules in the training set have errors less than 4 while the remaining 7 have errors less than 10. Figure 2A–C illustrates the selected Hypo1 pharmacophore model, while parts D, E, and F of Figure 2 show the mapping of compounds **1c**, **1d**, and **2h** onto Hypo1, respectively.

In compound **1c**, as seen in Figure 2D, the aromatic ring of the benzooxazolone moiety matches one of the HYAr features; the other HYAr feature is nicely overlapped by the additional phenyl ring. The carbonyl group and the basic nitrogen atom of the piperidine ring match the HBA and PI functions, while the chlorine atom on the monosubstituted phenyl ring maps the remaining HY feature. Quite an analogous mapping is observed for **1d** (Figure 2E). The estimated affinities for **1c** and **1d** are 0.27 and 280 nM, while the corresponding experimental affinities are 0.098 and 258 nM, respectively.

Figure 2F is an example of a pharmacophore mapping of a compound that is less active than the former two. Compound **2h** does not map all the features encoded in Hypo1. In fact, **2h** maps the two HYAr functions, again by means of the two phenyl rings; the PI feature is still overlapped by the nitrogen atom of the cyclic/linear bridging moiety, and the HBA function is located over the carbonyl oxygen. However, it does not map the HY function. According to this partial mapping, this compound is predicted to be less active.

A critical step in automated pharmacophore generation is model validation, especially in those cases where the model has been generated for the purpose of predicting the activity of external sets of compounds or, as in our case, of estimating the activity of newly conceived molecular entities prior to their synthesis. The first method we used to check the robustness of our correlation was the prediction of the affinity of a further set of molecules, also called the test set, composed of six additional molecules from our series and three compounds taken from the literature⁴² (see Table 5). The aim of this validation was to verify if our 3D pharmacophore model was able to predict the experimentally

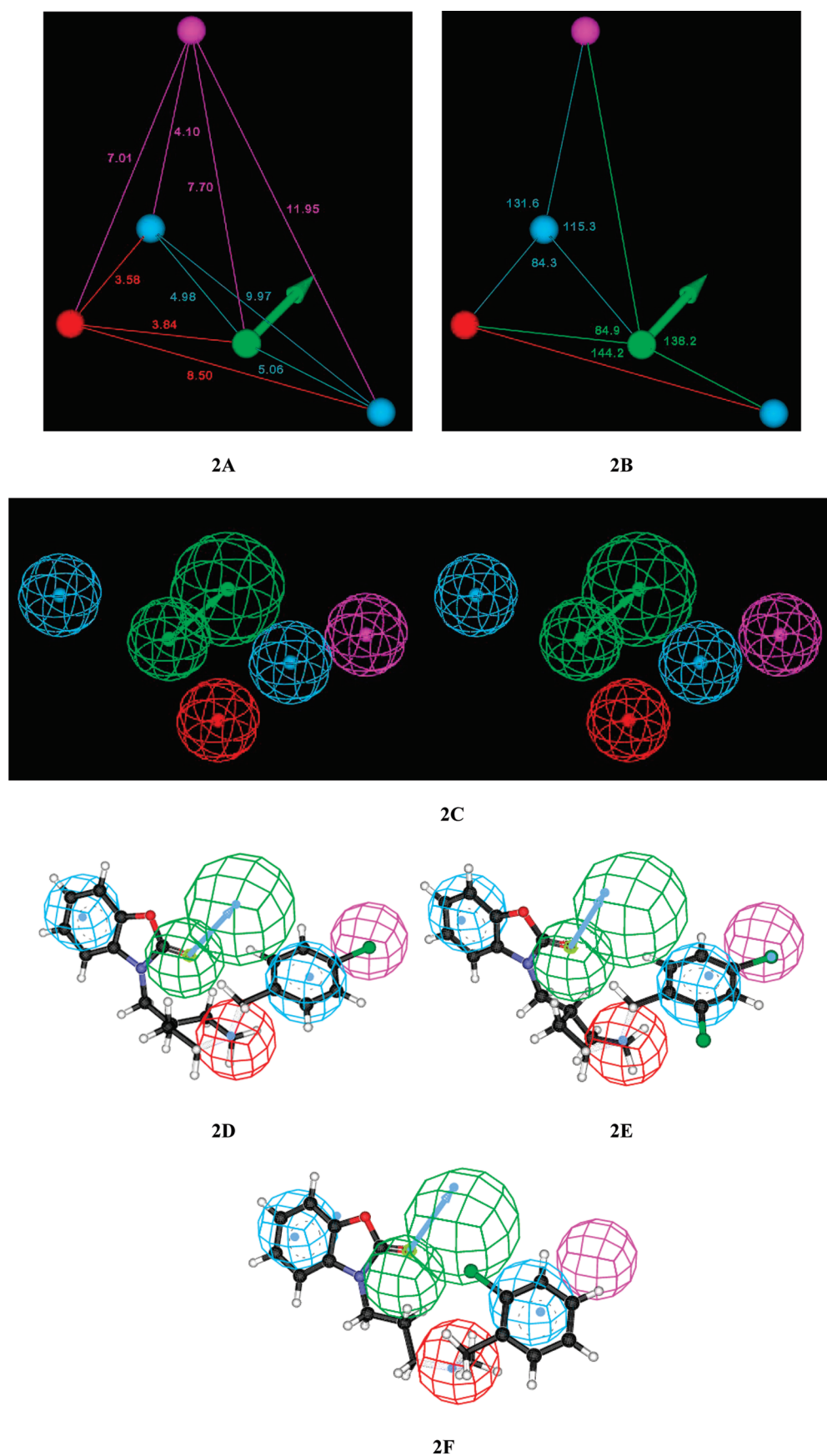


Figure 2. Geometrical relationships (A, B) among the features of the top-scoring pharmacophore Hypo1 (C, parallel glaze stereoview), and pharmacophore mapping of **1c** (D), **1d** (E), and **2h** (F) in the training set. The hypothesis features are portrayed as meshed spheres, color-coded as follows: red, PI; light blue, HYAr; pink, HY; light green, HBA. HBA is actually represented as a pair of spheres (the smaller sphere represents the location of the HBA atom on the ligand and the larger one the location of an HB donor on the receptor). Selected distances (Å) and angles (deg) are labeled.

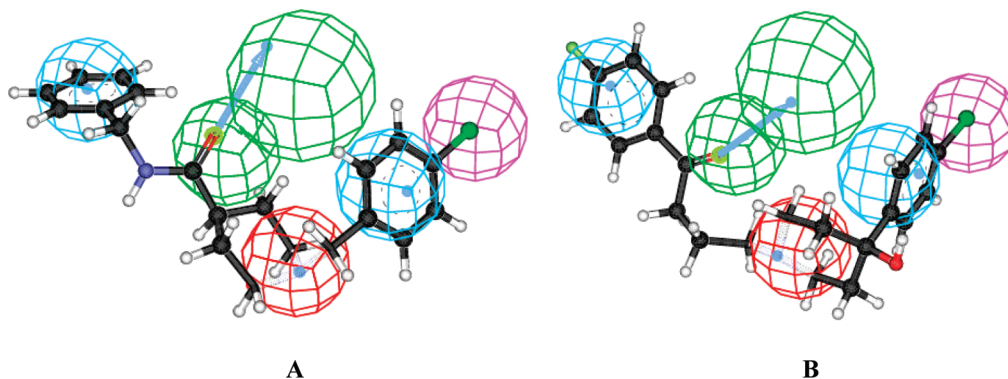


Figure 3. Pharmacophore mapping of **7b** (A) and **12** (B) in the test set. The hypothesis features are portrayed as meshed spheres, color-coded as follows: red, PI; light blue, HYAr; pink, HY; light green, HBA.

determined affinity values of the test set compounds. Interestingly, a good correlation coefficient (0.882) was observed when a regression analysis was performed by mapping the test set onto the features of the best pharmacophore hypothesis Hypo1. The predicted and the experimental K_i values for the test set along with the respective errors are shown in Table 5. The average error in predicting the affinity of the test set molecules is 2.5. Given the inherent simplicity of the pharmacophoric approach and considering the intrinsic variability of the biological responses, we can conclude that the ability of the present 3D pharmacophore model to predict the affinity of this series of σ_1 receptor ligands is quite satisfactory. Figure 3 shows the mapping of two test set molecules (**7b** and **12**, respectively) to the σ_1 receptor pharmacophore model. For both compounds, the two phenyl groups match the HYAr functions, the chlorine atom fits the HY feature, the carbonyl oxygen atom provides the HBA function, and the basic nitrogen is located over the PI feature.

Notwithstanding these good results, a second test was performed to check the statistical significance of the 3D pharmacophore model Hypo1, based on a randomization procedure. This was derived from the Fisher method using the CatScramble program available in the Catalyst suite of programs. According to the validation procedure, the experimental affinities of the compounds in the training set were scrambled randomly and the resulting new training sets were used for a number of new HypoGen runs. The parameters used in running these calculations were the same employed in the initial HypoGen calculation, and since a 98% confidence level was selected, 49 random hypothesis runs were performed. The results clearly indicate that randomization produced hypotheses with no predictive values similar or close to the corresponding Hypo1. Indeed, none of the outcome hypotheses had a lower cost score, better correlation, or smaller root-mean-square deviation than the initial hypothesis. Table 6 lists the first 10 lowest total score values of the resulting 49 hypotheses for our test set molecules. In conclusion, there is a 98% chance for the best hypothesis to represent a true correlation in the training set affinity data for the present classes of compounds.

Finally, a further statistical test, the leave-one-out method, which consists of recomputing the hypothesis by excluding from the training set one molecule at a time, was carried out. Basically, this test is performed to verify whether or not the correlation is strongly dependent on one particular compound in the training set. The test is positive if the

Table 6. Output Parameters of the 10 Lowest Cost Hypotheses Resulting from the Statistical Evaluation According to the CatScramble Validation Procedure for the σ_1 Receptor Ligands

hypothesis	ρ	rmsd	total cost
1	0.801	1.142	149.3
2	0.744	1.492	151.6
3	0.764	1.456	152.3
4	0.625	1.768	154.8
5	0.613	1.778	157.1
6	0.611	1.783	158.2
7	0.588	1.812	160.0
8	0.578	1.823	161.3
9	0.566	1.844	165.1
10	0.501	1.899	168.9
Hypo1	1.126	0.896	124.1

affinity of each excluded molecule is correctly predicted by the corresponding one-missing hypothesis. The value of ρ , the feature composition of the pharmacophore, and the quality of the predicted affinity of the excluded molecule were used as measures for the assessment of the statistical test. For each of the 31 new hypotheses generated according to this method, we did not obtain meaningful differences between Hypo1 and each hypothesis resulting from the exclusion of one compound at a time.

Overall, the 3D pharmacophore model derived in the present work is quite simple, and it is in perfect agreement with another pharmacophore model for σ_1 receptors previously reported by Glennon et al.,³⁴ in which a basic nitrogen is placed between two hydrophobic sites. Importantly, the primary hydrophobic site of Glennon's model is located at an optimum distance of 7–9 Å from the basic nitrogen. This corresponds well to our aromatic and aliphatic hydrophobic feature spheres (8.5 and 7.0 Å from the PI feature, respectively; see Figure 2C). The second hydrophobic site, reported at a distance of 2.5–3.9 Å from the basic nitrogen in Glennon's model, is matched by the remaining HYAr, which is located at 3.6 Å from the PI feature in our 3D pharmacophore. Also, our model compares well, both in terms of feature type and geometrical characteristics, with a more general pharmacophore model recently obtained by Laggner et al. for σ_1 and the ERG2 protein.⁴² As a concluding comment, we emphasize that only five-feature pharmacophore hypotheses were generated by Catalyst according to our procedure. This is significant for a number of reasons, first, because most prior published pharmacophores for σ_1 receptors contain only four features (as reviewed above), second, because our five-feature hypothesis does indeed

represent a more stringent and significant model, and last, because it illustrates that Catalyst identified sufficient evidence in this structural data set to add or distinguish an additional feature or nuance not seen previously.

Conclusions

In this work we discussed how, from three series of newly synthesized compounds characterized by a broad range of affinity toward σ_1 receptors, we derived a three-dimensional pharmacophore model with quantitative predictive ability for these classes of molecules. The best generated pharmacophore model (Hypo1) consists of five features: two hydrophobic aromatic, one hydrophobic aliphatic, one hydrogen bond acceptor, and one positive ionizable group. Hypo1 reasonably predicts the affinity of the test set molecules with a correlation coefficient of 0.896 and shows the best statistical significance among all the generated models. Two validation tests, the Fisher test and the leave-one-out test, confirmed the statistical validity of our simple but effective 3D pharmacophore, excluding any possibility of a chance correlation between experimental and predicted affinity values. Finally, the model was predictive not only for the training set compounds but also for a test set of nine additional molecules, three of which were taken from the literature and not structurally related to our series.

Compared with other drug discovery tools, the pharmacophore approach has the significant advantage that it is fast and able to predict the activity of quite a large number of molecules in a relatively short time. Given the reasonable predictive ability of our model, we expect to exploit it in the development and optimization of our promising series of compounds. In particular, we will use this 3D pharmacophore to estimate the potential affinity of virtual libraries of newly designed, second generation σ_1 receptor ligands prior to synthesis and biological testing.

Experimental Section

Unless otherwise noted, starting materials and reagents were obtained from commercial suppliers and were used without purification. Melting points were determined with a Buchi 510 capillary apparatus and are uncorrected. Infrared spectra in Nujol mulls were recorded on a Jasco FT 200 spectrophotometer. Proton nuclear magnetic resonance (^1H NMR) spectra were determined on a Varian Gemini 200 spectrometer, and the chemical shifts are reported as δ (ppm) in CDCl_3 solution. Coupling constants J are expressed in hertz (Hz). Reaction courses and product mixtures were routinely monitored by thin-layer chromatography (TLC) on silica gel precoated F₂₅₄ Merck plates. ESI-MS spectra were obtained on a PE-API I spectrometer by infusion of a solution of the sample in MeOH. Elemental analyses (C, H, N) were performed on a Carlo Erba 1106 analyzer and were within ± 0.3 of the theoretical value.

Synthesis of Benzoxazolone Derivatives. 3-(3-Chloropropyl)-benzo[d]oxazol-2(3H)-one (5a).⁴³ A mixture of benzo[d]oxazol-2(3H)-one **4** (3.0 g, 22.22 mmol) and K_2CO_3 (7.7 g, 55.55 mmol) was dissolved in 50 mL of CH_3CN and the solution was refluxed for 10 min. 1-Bromo-3-chloropropane (8.7 g, 55.55 mmol) and a catalytic amount of KI were added, and the mixture was stirred for an additional 3 h at reflux temperature. The inorganic salts were filtered off, and the solvent was evaporated under reduced pressure. Distilled water (50 mL) was added, and the residue was extracted 3 times with CHCl_3 (3×100 mL). The organic phase was separated and dried over anhydrous Na_2SO_4 . The filtered solution was concentrated under reduced pressure, and the remaining oil was crystallized from *n*-hexane to afford a light-yellow

solid. Yield 4.01 g (85%); mp 62–64 °C. IR (Nujol): 1791 cm^{-1} . ^1H NMR (CDCl_3 -TMS) ppm (δ): 2.30 (m, 2H, CH_2 - CH_2 - CH_2 , $J = 5.9$ –6.6 Hz); 3.63 (t, N- CH_2 , $J = 6.6$ Hz); 4.00 (t, 2H, CH_2 -Cl, $J = 5.9$ Hz); 7.00–7.30 (m, 4H arom). MS: m/z 212 [MH^+] 214 [$\text{MH}^+ + 2$].

3-(4-Bromobutyl)benzo[d]oxazol-2(3H)-one (5b).⁴⁴ This intermediate was obtained in an analogous way using 1,4-dibromobutane. Yield 2.99 g (60%); mp 42–45 °C. IR (Nujol): 1747 cm^{-1} . ^1H NMR (CDCl_3 -TMS) ppm (δ): 1.80 (m, 4H, CH_2 - CH_2 - CH_2); 3.63 (m, N- CH_2); 4.00 (m, 2H, CH_2 -Br); 7.10–7.40 (m, 4H arom). MS: m/z 270 [MH^+] 272 [$\text{MH}^+ + 2$].

3-[3-(*N*-Benzyl-*N*-methylamino)propyl]benzo[d]oxazol-2(3H)-one (2a). A mixture of 3-(4-chloropropyl)benzo[d]oxazol-2(3H)-one (0.60 g, 2.84 mmol), *N*-methylbenzylamine (0.28 g, 2.27 mmol), anhydrous K_2CO_3 (2.19 g, 15.9 mmol), and a catalytic amount of KI was dissolved in 50 mL of CH_3CN , and the solution was refluxed and monitored by TLC. The inorganic salts were filtered off, and the solvent was evaporated under reduced pressure. Distilled water (50 mL) was added, and the residue was extracted 3 times with CHCl_3 (3×100 mL). The organic phase was separated and dried over anhydrous Na_2SO_4 . The filtered solution was concentrated under reduced pressure and the remaining oil was treated with an equimolar amount of oxalic acid in absolute ethanol to yield the oxalate salt, which was filtered and washed with cold ethanol. Yield 0.26 g (0.20 g of free base, 30%); mp 180–182 °C. IR (Nujol): 1772, 2697 cm^{-1} . ^1H NMR (free base, CDCl_3 -TMS) ppm (δ): 2.01 (m, 2H, CH_2 - CH_2 - CH_2 , $J = 6.7$ –7.3 Hz); 2.21 (s, 3H, N- CH_3); 2.49 (t, 2H, CH_2 -N(CH_3)- CH_2 -Ar, $J = 6.7$ Hz); 3.51 (s, 2H, N- CH_2 -Ar); 3.93 (t, 2H, N- CH_2 -(CH_2)₂, $J = 7.3$ Hz); 6.95–7.40 (m, 9H, arom). MS: m/z 297 [MH^+].

Compounds **2b–k** were synthesized following the same route described above for compound **2a**.

3-[3-(*N*-(3-Chlorobenzyl)-*N*-methylamino)propyl]benzo[d]oxazol-2(3H)-one (2b). IR (Nujol): 1764, 2721 cm^{-1} . ^1H NMR (free base, CDCl_3 -TMS) ppm (δ): 1.97 (m, 2H, CH_2 - CH_2 - CH_2 , $J = 6.6$ –7.3 Hz); 2.15 (s, 3H, CH_3); 2.46 (t, 2H, CH_2 -N(CH_3)- CH_2 -Ar, $J = 6.6$ Hz); 3.51 (s, 2H, N- CH_2 -Ar); 3.84 (t, 2H, N- CH_2 -(CH_2)₂, $J = 7.3$ Hz); 6.89–7.37 (m, 8H, arom). MS: m/z 331 [MH^+] 333 [$\text{MH}^+ + 2$].

3-[3-(*N*-(3-Chlorobenzyl)-*N*-methylamino)propyl]benzo[d]oxazol-2(3H)-one (2c). IR (Nujol): 1767, 2673 cm^{-1} . ^1H NMR (free base, CDCl_3 -TMS) ppm (δ): 1.95 (m, 2H, CH_2 - CH_2 - CH_2 , $J = 6.6$ –7.3 Hz); 2.15 (s, 3H, CH_3); 2.45 (t, 2H, CH_2 -N(CH_3)- CH_2 -Ar, $J = 6.6$ Hz); 3.43 (s, 2H, N- CH_2 -Ar); 3.86 (t, 2H, N- CH_2 -(CH_2)₂, $J = 7.3$ Hz); 6.92–7.30 (m, 8H, arom). MS: m/z 331 [MH^+] 333 [$\text{MH}^+ + 2$].

3-[3-(*N*-(4-Chlorobenzyl)-*N*-methylamino)propyl]benzo[d]oxazol-2(3H)-one (2d). IR (Nujol): 1770, 2677 cm^{-1} . ^1H NMR (free base, CDCl_3 -TMS) ppm (δ): 2.05 (m, 2H, CH_2 - CH_2 - CH_2 , $J = 6.6$ –7.3 Hz); 2.17 (s, 3H, N- CH_3); 2.45 (t, 2H, CH_2 -N(CH_3)- CH_2 -Ar, $J = 6.6$ Hz); 3.46 (s, 2H, N- CH_2 -Ar); 3.90 (t, 2H, N- CH_2 -(CH_2)₂, $J = 7.3$ Hz); 6.95–7.30 (m, 8H, arom). MS: m/z 331 [MH^+] 333 [$\text{MH}^+ + 2$].

3-[3-(*N*-(2-Methoxybenzyl)-*N*-methylamino)propyl]benzo[d]oxazol-2(3H)-one (2e). IR (Nujol): 1771, 2673 cm^{-1} . ^1H NMR (free base, CDCl_3 -TMS) ppm (δ): 1.87–2.00 (m, 2H, CH_2 - CH_2 - CH_2 , $J = 6.6$ –7.3 Hz); 2.14 (s, 3H, CH_3); 2.43 (t, 2H, CH_2 -N(CH_3)- CH_2 -Ar, $J = 6.6$ Hz); 3.45 (s, 2H, N- CH_2 -Ar); 3.75 (s, 3H, OCH₃); 3.87 (t, 2H, N- CH_2 -(CH_2)₂, $J = 7.3$ Hz); 6.79–7.25 (m, 8H, arom). MS: m/z 327 [MH^+].

3-[3-(*N*-(3-Methoxybenzyl)-*N*-methylamino)propyl]benzo[d]oxazol-2(3H)-one (2f). IR (Nujol): 1770, 2676 cm^{-1} . ^1H NMR (free base, CDCl_3 -TMS) ppm (δ): 1.83–1.97 (m, 2H, CH_2 - CH_2 - CH_2 , $J = 6.6$ –7.3 Hz); 2.12 (s, 3H, CH_3); 2.40 (t, 2H, CH_2 -N(CH_3)- CH_2 -Ar, $J = 6.6$ Hz); 3.39 (s, 2H, N- CH_2 -Ar); 3.74 (s, 3H, OCH₃); 3.84 (t, 2H, N- CH_2 -(CH_2)₂, $J = 7.3$ Hz); 6.70–7.21 (m, 8H, arom). MS: m/z 327 [MH^+].

3-[3-(*N*-(4-Methoxybenzyl)-*N*-methylamino)propyl]benzo[d]oxazol-2(3H)-one (2g). IR (Nujol): 1771, 2685 cm^{-1} . ^1H NMR

(free base, CDCl_3 -TMS) ppm (δ): 1.98 (m, 2H, CH_2 - CH_2 - CH_2 , $J = 6.7$ – 7.3 Hz); 2.20 (s, 3H, CH_3); 2.43 (t, 2H, CH_2 - $\text{N}(\text{CH}_3)$ - CH_2 -Ar, $J = 6.7$ Hz); 3.45 (s, 2H, N- CH_2 -Ar); 3.84 (s, 3H, OCH_3); 3.91 (t, 2H, N- CH_2 -(CH_2)₂-, $J = 7.3$ Hz); 6.85–7.30 (m, 8H, arom). MS: m/z 327 [MH^+].

3-[3-[*N*-Methylamino-*N*-(2-methylbenzyl)]propyl]benzo[d]oxazol-2(3*H*)-one (2h). IR (Nujol): 1766, 2723 cm^{-1} . ^1H NMR (free base, CDCl_3 -TMS) ppm (δ): 1.82–1.96 (m, 2H, CH_2 - CH_2 - CH_2 , $J = 6.6$ – 7.3 Hz); 2.14 (s, 3H, CH_3); 2.30 (s, 3H, CH_3); 2.44 (t, 2H, CH_2 - $\text{N}(\text{CH}_3)$ - CH_2 -Ar, $J = 6.6$ Hz); 3.40 (s, 2H, N- CH_2 -Ar); 3.78 (t, 2H, N- CH_2 -(CH_2)₂-, $J = 7.3$ Hz); 6.86–7.23 (m, 8H, arom). MS: m/z 311 [MH^+].

3-[3-[*N*-Methylamino-*N*-(3-methylbenzyl)]propyl]benzo[d]oxazol-2(3*H*)-one (2i). IR (Nujol): 1770, 2676 cm^{-1} . ^1H NMR (free base, CDCl_3 -TMS) ppm (δ): 1.84–1.98 (m, 2H, CH_2 - CH_2 - CH_2 , $J = 6.6$ – 7.3 Hz); 2.12 (s, 3H, CH_3); 2.26 (s, 3H, CH_3); 2.40 (t, 2H, CH_2 - $\text{N}(\text{CH}_3)$ - CH_2 -Ar, $J = 6.6$ Hz); 3.38 (s, 2H, N- CH_2 -Ar); 3.84 (t, 2H, N- CH_2 -(CH_2)₂-, $J = 7.3$ Hz); 6.91–7.18 (m, 8H, arom). MS: m/z 311 [MH^+].

3-[3-[*N*-Methylamino-*N*-(4-methylbenzyl)]propyl]benzo[d]oxazol-2(3*H*)-one (2j). IR (Nujol): 1766, 2675 cm^{-1} . ^1H NMR (free base, CDCl_3 -TMS) ppm (δ): 1.85–1.99 (m, 2H, CH_2 - CH_2 - CH_2 , $J = 6.6$ – 7.3 Hz); 2.14 (s, 3H, CH_3); 2.27 (s, 3H, CH_3); 2.42 (t, 2H, CH_2 - $\text{N}(\text{CH}_3)$ - CH_2 -Ar, $J = 6.6$ Hz); 3.43 (s, 2H, N- CH_2 -Ar); 3.82 (t, 2H, N- CH_2 -(CH_2)₂-, $J = 7.3$ Hz); 6.92–7.20 (m, 8H, arom). MS: m/z 311 [MH^+].

3-[3-[*N*-(2,4-Dimethylbenzyl)-*N*-methylamino]propyl]benzo[d]oxazol-2(3*H*)-one (2k). IR (Nujol): 1777, 2725 cm^{-1} . ^1H NMR (free base, CDCl_3 -TMS) ppm (δ): 1.97 (m, 2H, CH_2 - CH_2 - CH_2 , $J = 6.7$ – 7.3 Hz); 2.21 (s, 3H, N- CH_3); 2.33 (s, 3H, CH_3); 2.35 (s, 3H, CH_3); 2.50 (t, 2H, CH_2 - $\text{N}(\text{CH}_3)$ - CH_2 -Ar, $J = 6.7$ Hz); 3.43 (s, 2H, N- CH_2 -Ar); 3.86 (t, 2H, N- CH_2 -(CH_2)₂-, $J = 7.3$ Hz); 6.95–7.30 (m, 7H, arom). MS: m/z 325 [MH^+].

3-[4-(*N*-Benzyl-*N*-methylamino)butyl]benzo[d]oxazol-2(3*H*)-one (3a). A mixture of 3-(4-bromobutyl)benzo[d]oxazol-2(3*H*)-one (0.25 g, 0.926 mmol), *N*-methylbenzylamine (0.089 g, 0.741 mmol), anhydrous K_2CO_3 (0.72 g, 5.19 mmol), and a catalytic amount of KI was dissolved in 50 mL of ACN, and the solution was refluxed and monitored by TLC. The inorganic salts were filtered off, and the solvent was evaporated under reduced pressure. Distilled water (50 mL) was added, and the residue was extracted 3 times with CHCl_3 (3 \times 100 mL). The organic phase was separated and dried over anhydrous Na_2SO_4 . The filtered solution was concentrated under reduced pressure and the remaining oil was treated with an equimolar amount of oxalic acid in absolute ethanol to afford the oxalate salt, which was filtered and washed with cold ethanol. Yield 0.12 g (0.09 g of free base, 30%); mp 145–150 $^\circ\text{C}$. IR (Nujol): 1772, 2668 cm^{-1} . ^1H NMR (free base, CDCl_3 -TMS) ppm (δ): 1.50–2.00 (m, 4H, CH_2 - CH_2 - CH_2 - CH_2 , $J = 6.7$ – 7.3 Hz); 2.20 (s, 3H, N- CH_3); 2.40 (t, 2H, CH_2 - $\text{N}(\text{CH}_3)$ - CH_2 -Ar, $J = 6.7$ Hz); 3.45 (s, 2H, N- CH_2 -Ar); 3.85 (t, 2H, N- CH_2 -(CH_2)₃-, $J = 7.3$ Hz); 6.90–7.40 (m, 9H, arom). MS: m/z 311 [MH^+].

Compounds **3b–k** were synthesized following the same route describe above for compound **3a**.

3-[4-[*N*-(2-Chlorobenzyl)-*N*-methylamino]butyl]benzo[d]oxazol-2(3*H*)-one (3b). IR (Nujol): 1770, 2674 cm^{-1} . ^1H NMR (CDCl_3 -TMS) ppm (δ): 1.49–1.90 (m, 4H, CH_2 - CH_2 - CH_2 - CH_2); 2.13 (s, 3H, CH_3); 2.39 (t, 2H, CH_2 - $\text{N}(\text{CH}_3)$ - CH_2 -Ar, $J = 6.6$ Hz); 3.40 (s, 2H, N- CH_2 -Ar); 3.81 (t, 2H, N- CH_2 -(CH_2)₃-, $J = 7.3$ Hz); 6.90–7.25 (m, 8H, arom). MS: m/z 345 [MH^+] 347 [$\text{MH}^+ + 2$].

3-[4-[*N*-(3-Chlorobenzyl)-*N*-methylamino]butyl]benzo[d]oxazol-2(3*H*)-one (3c). IR (Nujol): 1766, 2670 cm^{-1} . ^1H NMR (CDCl_3 -TMS) ppm (δ): 1.49–1.90 (m, 4H, CH_2 - CH_2 - CH_2 - CH_2); 2.14 (s, 3H, CH_3); 2.39 (t, 2H, CH_2 - $\text{N}(\text{CH}_3)$ - CH_2 -Ar, $J = 6.6$ Hz); 3.40 (s, 2H, N- CH_2 -Ar); 3.82 (t, 2H, N- CH_2 -(CH_2)₃-, $J = 7.3$ Hz); 6.91–7.27 (m, 8H, arom). MS: m/z 345 [MH^+] 347 [$\text{MH}^+ + 2$].

3-[4-[*N*-(4-Chlorobenzyl)-*N*-methylamino]butyl]benzo[d]oxazol-2(3*H*)-one (3d). IR (Nujol): 1768, 2676 cm^{-1} . ^1H NMR (CDCl_3 -TMS) ppm (δ): 1.50–1.65 (m, 2H, CH_2 - CH_2 - CH_2);

1.75–1.90 (m, 2H, CH_2 - CH_2 - CH_2); 2.15 (s, 3H, CH_3); 2.36–2.43 (t, 2H, CH_2 - $\text{N}(\text{CH}_3)$ - CH_2 -Ar, $J = 6.6$ Hz); 3.42 (s, 2H, N- CH_2 -Ar); 3.79–3.86 (t, 2H, N- CH_2 -(CH_2)₃-, $J = 7.3$ Hz); 6.93–7.29 (m, 8H, arom). MS: m/z 345 [MH^+] 347 [$\text{MH}^+ + 2$].

3-[4-[*N*-(2-Methoxybenzyl)-*N*-methylamino]butyl]benzo[d]oxazol-2(3*H*)-one (3e). IR (Nujol): 1770, 2673 cm^{-1} . ^1H NMR (CDCl_3 -TMS) ppm (δ): 1.53–1.90 (m, 4H, CH_2 - CH_2 - CH_2 - CH_2); 2.20 (s, 3H, CH_3); 2.45 (t, 2H, CH_2 - $\text{N}(\text{CH}_3)$ - CH_2 -Ar, $J = 6.6$ Hz); 3.48 (s, 2H, N- CH_2 -Ar); 3.79 (s, 3H, CH_3); 3.87 (t, 2H, N- CH_2 -(CH_2)₃-, $J = 7.3$ Hz); 6.83–7.30 (m, 8H, arom). MS: m/z 341 [MH^+].

3-[4-[*N*-(3-Methoxybenzyl)-*N*-methylamino]butyl]benzo[d]oxazol-2(3*H*)-one (3f). IR (Nujol): 1769, 2674 cm^{-1} . ^1H NMR (CDCl_3 -TMS) ppm (δ): 1.54–1.91 (m, 2H, CH_2 - CH_2 - CH_2 - CH_2); 2.19 (s, 3H, CH_3); 2.44 (t, 2H, CH_2 - $\text{N}(\text{CH}_3)$ - CH_2 -Ar, $J = 6.6$ Hz); 3.49 (s, 2H, N- CH_2 -Ar); 3.79 (s, 3H, CH_3); 3.86 (t, 2H, N- CH_2 -(CH_2)₃-, $J = 7.3$ Hz); 6.81–7.28 (m, 8H, arom). MS: m/z 341 [MH^+].

3-[3-[*N*-(4-Methoxybenzyl)-*N*-methylamino]butyl]benzo[d]oxazol-2(3*H*)-one (3g). IR (Nujol): 1774, 2724 cm^{-1} . ^1H NMR (free base, CDCl_3 -TMS) ppm (δ): 1.53–1.90 (m, 4H, CH_2 - CH_2 - CH_2 - CH_2 , $J = 6.7$ – 7.3 Hz); 2.18 (s, 3H, CH_3); 2.40 (t, 2H, CH_2 - $\text{N}(\text{CH}_3)$ - CH_2 -Ar, $J = 6.7$ Hz); 3.42 (s, 2H, N- CH_2 -Ar); 3.86 (m, 5H, OCH_3 and N- CH_2 -(CH_2)₃-, $J = 7.3$ Hz); 6.84–7.30 (m, 8H, arom). MS: m/z 341 [MH^+].

3-[4-(*N*-Methylamino-*N*-(2-methylbenzyl)]benzo[d]oxazol-2(3*H*)-one (3h). IR (Nujol): 1769, 2668 cm^{-1} . ^1H NMR (CDCl_3 -TMS) ppm (δ): 1.49–1.90 (m, 4H, CH_2 - CH_2 - CH_2 - CH_2); 2.15 (s, 3H, CH_3); 2.33 (s, 3H, CH_3); 2.41 (t, 2H, CH_2 - $\text{N}(\text{CH}_3)$ - CH_2 -Ar, $J = 6.6$ Hz); 3.41 (s, 2H, N- CH_2 -Ar); 3.79 (t, 2H, N- CH_2 -(CH_2)₃-, $J = 7.3$ Hz); 6.89–7.25 (m, 8H, arom). MS: m/z 325 [MH^+].

3-[4-(*N*-Methylamino-*N*-(3-methylbenzyl)]benzo[d]oxazol-2(3*H*)-one (3i). IR (Nujol): 1770, 2666 cm^{-1} . ^1H NMR (CDCl_3 -TMS) ppm (δ): 1.50–1.91 (m, 4H, CH_2 - CH_2 - CH_2 - CH_2); 2.15 (s, 3H, CH_3); 2.31 (s, 3H, CH_3); 2.38 (t, 2H, CH_2 - $\text{N}(\text{CH}_3)$ - CH_2 -Ar, $J = 6.6$ Hz); 3.40 (s, 2H, N- CH_2 -Ar); 3.81 (t, 2H, N- CH_2 -(CH_2)₃-, $J = 7.3$ Hz); 6.92–7.22 (m, 8H, arom). MS: m/z 325 [MH^+].

3-[4-(*N*-Methylamino-*N*-(4-methylbenzyl)]benzo[d]oxazol-2(3*H*)-one (3j). IR (Nujol): 1769, 2674 cm^{-1} . ^1H NMR (CDCl_3 -TMS) ppm (δ): 1.51–1.92 (m, 4H, CH_2 - CH_2 - CH_2 - CH_2); 2.16 (s, 3H, CH_3); 2.33 (s, 3H, CH_3); 2.39 (t, 2H, CH_2 - $\text{N}(\text{CH}_3)$ - CH_2 -Ar, $J = 6.6$ Hz); 3.43 (s, 2H, N- CH_2 -Ar); 3.82 (t, 2H, N- CH_2 -(CH_2)₃-, $J = 7.3$ Hz); 6.93–7.23 (m, 8H, arom). MS: m/z 325 [MH^+].

3-[4-[*N*-(2,4-Dimethylbenzyl)-*N*-methylamino]butyl]benzo[d]oxazol-2(3*H*)-one (3k). IR (Nujol): 1779, 2724 cm^{-1} . ^1H NMR (free base, CDCl_3 -TMS) ppm (δ): 1.50–1.88 (m, 4H, CH_2 - CH_2 - CH_2 - CH_2 , $J = 6.7$ – 7.3 Hz); 2.17 (s, 3H, N- CH_3); 2.32 (s, 6H, 2 \times CH_3); 2.42 (t, 2H, CH_2 - $\text{N}(\text{CH}_3)$ - CH_2 -Ar, $J = 6.7$ Hz); 3.40 (s, 2H, N- CH_2 -Ar); 3.82 (t, 2H, N- CH_2 -(CH_2)₃-, $J = 7.3$ Hz); 6.90–7.30 (m, 7H, arom). MS: m/z 341 [MH^+].

Synthesis of Carboxamide Derivatives. *N*-Phenyl-1-(*tert*-butoxycarbonyl)piperidine-4-carboxamide (8).⁴⁵ To a mixture of *N*-Boc-4-piperidinecarboxylic acid (2.12 g, 9.22 mmol), pyridine (1.90 mL, 23.6 mmol) and CH_2Cl_2 (15 mL) and SOCl_2 (0.80 mL, 11.0 mmol) were added, under N_2 at room temperature, while stirring. After 25 min, a solution of aniline (0.95 g, 10.2 mmol), Et_3N (4.50 mL, 32.3 mmol), and a catalytic amount of DMAP in CH_2Cl_2 (15 mL) was added dropwise. The reaction was monitored by TLC. After 14 h, the organic phase was washed with 1 N HCl (2 \times 20 mL) and distilled water (2 \times 20 mL), dried with Na_2SO_4 , and concentrated in vacuum to give 1.70 g (60.1%) of a light-brown solid; mp 140–142 $^\circ\text{C}$. IR (Nujol): 1656, 1685, 3257 cm^{-1} . ^1H NMR (CDCl_3 -TMS) ppm (δ): 1.44 (s 9H, CH_3 , Boc); 1.60–1.93 (m, 4H, $\text{H}_{3,3'}$ - $\text{H}_{5,5'}$, pip.); 2.36 (m, 1H, H_4 , pip.); 2.76 (m, 2H, H_2 - H_6 , pip.); 4.17 (m, 2H, H_2 - H_6 , pip.); 7.05–7.52 (m, 6H, arom + NH disappearing on deuteration). MS: m/z 305 [MH^+].

Compound **9** was synthesized in analogous way using benzylamine instead of aniline. Yield: 1.52 g (52%).

***N*-Benzyl-1-(*tert*-butoxycarbonyl)piperidine-4-carboxamide (9).** IR (Nujol): 1634, 1681, 3251 cm^{-1} . ^1H NMR (CDCl_3 -TMS)

ppm (δ): 1.38 (s, 9H, CH₃, Boc); 1.45–1.77 (m, 4H, H_{3,3'}-H_{5,5'}, pip.); 2.21 (m, 1H, H₄, pip.); 2.65 (m, 2H, H₂-H₆, pip.); 4.06 (m, 2H, H_{2'}-H_{6'}, pip.); 4.36 (s, 2H, Ar-CH₂-N-CO); 5.90 (s broad, 1H, NH, disappearing on deuteration); 7.08–7.30 (m, 5H, arom). MS: m/z 319 [MH⁺].

N-Phenylpiperidine-4-carboxamide (10).⁴⁶ Compound **8** (1.00 g, 3.24 mmol) was deprotected with 2 mL of trifluoroacetic acid at room temperature for 24 h. The solution was concentrated at reduced pressure, and the residue was poured into water and basified with NaOH 10% solution (pH 10). The mixture was extracted with AcOEt (3 \times 25 mL). The organic phase was dried with Na₂SO₄ and concentrated. The obtained solid was used without further purification. Yield: 0.60 g (89%); mp 105–107 °C. IR (Nujol): 1655, 3258 cm⁻¹. ¹H NMR (CDCl₃-TMS) ppm (δ): 1.57–1.96 (m, 5H, H_{3,3'}-H_{5,5'}, pip. + NH disappearing on deuteration); 2.33 (m, 1H, H₄, pip.); 2.57 (m, 2H, H₂-H₆, pip.); 3.13 (m, 2H, H_{2'}-H_{6'}, pip.); 7.04–7.50 (m, 6H, arom + NH disappearing on deuteration). MS: m/z 205 [MH⁺].

Compound **11** was synthesized starting from **9** (1.2 g) using the same procedure. Yield: 0.75 g (91%); mp 115–117 °C.

N-Benzylpiperidine-4-carboxamide (11).⁴⁷ IR (Nujol): 1634, 3248 cm⁻¹. ¹H NMR (CDCl₃-TMS) ppm (δ): 1.50–1.78 (m, 4H, H_{3,3'}-H_{5,5'}, pip.); 2.11–2.26 (m, 2H, H₄, pip. + NH disappearing on deuteration); 2.52 (m, 2H, H₂-H₆, pip.); 3.05 (m, 2H, H_{2'}-H_{6'}, pip.); 4.32 (s, 2H, Ar-CH₂-N-CO); 6.13 (s broad, 1H, NH, disappearing on deuteration); 7.10–7.34 (m, 5H, arom). MS: m/z 219 [MH⁺].

1-Benzyl-N-phenylpiperidine-4-carboxamide (6a). A solution of **10** (0.17 g, 0.84 mmol), K₂CO₃ (0.14 g, 1.00 mmol), and benzyl chloride (0.11 g, 0.84 mmol) in 50 mL of acetone was stirred under reflux for 5 h. After the mixture was cooled, the inorganic salt was filtered and the solvent evaporated at reduced pressure. The residue was washed with distilled water and then with ethyl ether to afford **6a** as a chromatographically pure solid: yield 0.18 g (66%); mp 138–140 °C. IR (Nujol): 1657, 3318 cm⁻¹. ¹H NMR (CDCl₃-TMS) ppm (δ): 1.80–2.32 (m, 7H, H₂-H_{3,3'}-H_{5,5'}-H₆-H₄, pip.); 3.02 (m, 2H, H_{2'}-H_{6'}, pip.); 3.57 (s, 2H, N-CH₂-Ar); 7.06–7.55 (m, 11H, arom + NH disappearing on deuteration). MS: m/z 295 [MH⁺].

Compounds **6b** and **6c** were synthesized according to the procedure reported above. Compounds **7a**, **7b**, and **7c** were also synthesized following the same route but starting from **11**.

N-Phenyl-1-(4-chlorobenzyl)piperidine-4-carboxamide (6b). IR (Nujol): 1656, 3301 cm⁻¹. ¹H NMR (CDCl₃-TMS) ppm (δ): 1.63–2.26 (m, 7H, H₂-H_{3,3'}-H_{5,5'}-H₆-H₄, pip.); 2.93 (m, 2H, H_{2'}-H_{6'}, pip.); 3.47 (s, 2H, N-CH₂-Ar); 7.06–7.53 (m, 10H, arom + NH disappearing on deuteration). MS: m/z 329 [MH⁺] 331 [MH⁺ + 2].

N-Phenyl-1-(4-methylbenzyl)piperidine-4-carboxamide (6c). IR (Nujol): 1654, 3292 cm⁻¹. ¹H NMR (CDCl₃-TMS) ppm (δ): 1.62–2.29 (m, 7H, H₂-H_{3,3'}-H_{5,5'}-H₆-H₄, pip.); 2.34 (s, 3H, CH₃); 2.97 (m, 2H, H_{2'}-H_{6'}, pip.); 3.48 (s, 2H, N-CH₂-Ar); 7.10–7.53 (m, 10H, arom + NH disappearing on deuteration). MS: m/z 309 [MH⁺].

N,1-Dibenzylpiperidine-4-carboxamide (7a).⁴⁸ IR (Nujol): 1634, 3248 cm⁻¹. ¹H NMR (CDCl₃-TMS) ppm (δ): 1.65–2.13 (m, 7H, H₂-H_{3,3'}-H_{5,5'}-H₆-H₄, pip.); 2.84 (m, 2H, H_{2'}-H_{6'}, pip.); 3.40 (s, 2H, N-CH₂-Ar); 4.40 (s, 2H, Ar-CH₂-N-CO); 5.75 (s broad, 1H, NH, disappearing on deuteration); 7.13–7.36 (m, 10H, arom). MS: m/z 309 [MH⁺].

N-Benzyl-1-(4-chlorobenzyl)piperidine-4-carboxamide (7b). IR (Nujol): 1633, 3247 cm⁻¹. ¹H NMR (CDCl₃-TMS) ppm (δ): 1.62–2.20 (m, 7H, H₂-H_{3,3'}-H_{5,5'}-H₆-H₄, pip.); 2.87 (m, 2H, H_{2'}-H_{6'}, pip.); 3.43 (s, 2H, N-CH₂-Ar); 4.37 (s, 2H, Ar-CH₂-N-CO); 5.78 (s broad, 1H, NH, disappearing on deuteration); 7.14–7.32 (m, 9H, arom). MS: m/z 343 [MH⁺] 345 [MH⁺ + 2].

N-Benzyl-1-(4-methylbenzyl)piperidine-4-carboxamide (7c). IR (Nujol): 1636, 3251 cm⁻¹. ¹H NMR (CDCl₃-TMS) ppm (δ): 1.80–2.29 (m, 7H, H₂-H_{3,3'}-H_{5,5'}-H₆-H₄, pip.); 2.41 (s, 3H,

CH₃); 3.00 (m, 2H, H_{2'}-H_{6'}, pip.); 3.53 (s, 2H, N-CH₂-Ar); 4.51 (s, 2H, Ar-CH₂-N-CO); 5.84 (s broad, 1H, NH, disappearing on deuteration); 7.18–7.45 (m, 9H, arom). MS: m/z 323 [MH⁺].

Pharmacology. Radioligand Binding Assays. Binding assays were performed on rat liver membranes according to the methods of Hellewell²³ and were slightly modified as previously described.³³ Briefly, for the σ_1 receptor assay 250 μ g of rat liver homogenate was incubated for 120 min at 37 °C with 1 nM [³H]-(+)-pentazocine (PerkinElmer, specific activity 34.9 Ci/mmol) in 50 mM Tris-HCl, pH 8.0, 0.5 mL final volume. Nonspecific binding was defined in the presence of 10 μ M haloperidol. The reaction was stopped by vacuum filtration through GF/B glass-fiber filters presoaked with 0.5% polyethylenimine, followed by rapid washing with 2 mL of ice-cold buffer. The filters were placed in 3 mL of scintillation cocktail, and the radioactivity was determined by liquid scintillation counting.

For the σ_2 receptor assay, 150 μ g of rat liver homogenate was incubated for 120 min at room temperature with 3 nM [³H]DTG (PerkinElmer, specific activity 58.1 Ci/mmol) in 50 mM Tris-HCl, pH 8.0, 0.5 mL final volume. (+)-Pentazocine (100 nM) and haloperidol (10 μ M) were used to mask σ_1 receptors and to define nonspecific binding, respectively.

Competition studies were done using at least 11 different concentrations of the ligand under investigation. As an internal control, three increasing concentrations of unlabeled (+)-pentazocine (σ_1 receptors) or DTG (σ_2 receptors) were always included. The compounds were prepared as 10 mM stock solutions in 100% DMSO and diluted with Tris-HCl buffer on the day of the experiment. The final DMSO concentration in the incubation tubes was maintained at 0.1%.

The competition data for two to four separate determinations performed in duplicate were averaged by fitting to a four-parameter curve by means of the SigmaPlot software. Calculated IC₅₀ values and Hill's coefficients (n_H) are reported as mean values \pm SEM. The corresponding K_i values were obtained by the Cheng-Prusoff equation, as previously reported.⁴⁹

Molecular Modeling. Training and Test Sets. The model structures of all compounds were built using the Catalyst 2D-3D sketcher.³⁸ High quality conformational models are crucial for the development of predictive pharmacophore models. Accordingly, in this study we employed an ad hoc procedure to derive molecular conformations, instead of using those generated by Catalyst, for better quality in covering the low-energy conformational space. Each molecular structure was subjected to energy minimization using the generalized CHARMM force field⁵⁰ until the gradient dropped below 0.05. The minimized structures were used as the starting point for subsequent conformational searches. A 10000-step Monte Carlo torsional sampling conformational search was conducted for each compound. Unique low-energy conformations within 20 kcal/mol of the corresponding global energy minimum were collected for each molecule. A conformation was considered unique only when the maximum displacement of at least one heavy atom was greater than 0.5 Å. A maximum of 250 unique conformations were recovered for each compound. The classical conformational search was also carried out using the Poling algorithm^{51–53} and the CHARMM force field⁵¹ as implemented in the Catalyst program for comparison. The “best quality” generation option was adopted to select representative conformers over a 0–20 kcal/mol interval above the computed global energy minimum in the conformational space, and again, the number of conformers generated for each compound was limited to a maximum of 250. Comparing the results of the two conformational searches, we verified the existence of considerable differences between the two approaches in generating conformations for saturated six-member rings such as piperidine. This group is quite common in drug molecules

and constitutes a popular molecular scaffold. A survey of the crystal structures of druglike molecules and protein/ligand complexes available in the literature and in public databases reveals that this saturated ring overwhelmingly adopts low-energy chair conformations. The conformational search conducted with the typical Catalyst settings described above, however, generated predominantly twisted conformations that might lead to an incorrect mapping of this functionally important group. In comparison, the alternative procedure of conformational search produced a considerable number of chair conformations for this heterocyclic moiety. The main drawback of this technique, however, is that it takes considerable longer to generate the relevant conformational models. Nonetheless, as the spirit of the work was the generation of a predictive 3D pharmacophore model for these classes of compounds, we considered it worthwhile to use more accurate conformational models.

On the basis of the conformations for each compound, the HypoGen module of the Catalyst 4.9 software package was used to generate three-dimensional pharmacophore models. During hypotheses generation, the software attempts to minimize a cost function containing two main terms: the first penalizes the deviation between the estimated affinities of the training set molecules and their experimental values, while the second penalizes the complexity of the hypothesis. The uncertainty factor for each compound represents the ratio range of uncertainty in the affinity value based on the expected statistical irregularity of biological data collection. Uncertainty influences the first step (also called the constructive phase) of the hypothesis generating process. In this work, an uncertainty of 1.1 was preferred over the default factor of 3.0, as the experimental affinities of our compounds barely span the required 4 orders of magnitude.

Briefly, a pharmacophore captures the three-dimensional arrangement of the structural features shared by all active molecules that are presumably essential for the desired pharmacological activity. These features include hydrogen bond donors (HBD) and acceptors (HBA), hydrophobic groups (HY), aromatic rings (RA), positively charged/ionizable groups (PC/PI), and negatively charged/ionizable (NC/NI) moieties. In addition, shape restraints and excluded volume effects can also be incorporated in the 3D-QSAR pharmacophores to account for the framework of the target active site. These popular modeling techniques find many practical applications in drug design. For instance, they can be used to align structurally unrelated lead compounds, thus identifying the groups in each molecular structure that play an important role for the corresponding biological activity. Moreover, the nonessential parts of the molecules can be altered to improve their physicochemical or pharmacokinetic properties, and new molecular scaffolds can be designed to establish novel patent space. Last but not least, pharmacophore models have been applied with success in virtual screening to extract molecular entities for biological activity testing from large, proprietary, or public databases.⁵⁴

An analysis of the functional groups characterizing our compounds suggested that hydrophobic aromatic (HYAr) and aliphatic (HYAl) features, hydrogen bond acceptors (HBA), positive ionizable (PI), and ring aromatic (RAr) features could effectively map the critical chemical features and hence describe the σ_1 receptor affinity of our compounds. Accordingly, these five features were selected to constitute the essential information in the automated hypothesis generation process.

Three validation procedures were used to determine the statistical relevance and the validity of the proposed 3D pharmacophore models: the test set prediction method, the CatScramble method, and the leave-one-out procedure. In this work, the first procedure consisted of a collection of further, different compounds into a test set and of performing a regression analysis by mapping the test set molecules onto

the best pharmacophore hypothesis. The high correlation coefficients obtained using the test set compounds revealed the good correlation between the actual and estimated affinities and hence the predictive validity of the corresponding 3D hypothesis. The CatScramble validation procedure is based on Fisher's randomization test.⁵⁵ The goal of this type of validation is to check whether there is a strong correlation between the chemical structures and the biological activity. This is done by randomizing the affinity data associated with the training set compounds, generating pharmacophore hypotheses using the same features and parameters employed to develop the original pharmacophore model. The statistical significance is calculated according to the following formula:

$$\text{significance} = 100 \times [1 - (1 + x/y)]$$

where x is the total number of hypotheses having a total cost lower than the original (best) hypothesis and y is the total number of HypoGen runs (initial + random runs). Thus, 49 random spreadsheets (i.e., 49 HypoGen runs) have to be generated to obtain a 98% confidence level. Should any randomized data set result in the generation of a 3D pharmacophore with similar or even better cost values, root-mean-square deviations, and correlation coefficients, then it is likely that the original hypothesis does reflect a chance correlation.

Finally, the leave-one-out test checks if the correlation between experimental and computed affinities is heavily dependent on one particular molecule of the training set by recomputing the pharmacophore model with the exclusion of one molecule at a time. Accordingly, 31 new training sets were derived, each composed of 30 molecules, and 31 HypoGen calculations were performed under the same conditions. For each run, the hypothesis characterized by the lowest total cost was employed to predict the affinity of the excluded compound and to estimate the new correlation coefficient.

All PDB structures and 3D hypotheses generated in this work are available from the authors upon request.

Acknowledgment. Financial support from the Italian Ministry of University and Scientific Research (MIUR, Rome) (Project PRIN-2005) is gratefully acknowledged. The authors thank Dr. Tien Luu for thoroughly reading the manuscript and her critical comments.

Supporting Information Available: Parameters for the 10 top hypotheses generated, elemental analysis results of compounds **2**, **3**, **6**, and **7**, and table with Hill coefficients for compounds **6a–c** and **7a–c**. This material is available free of charge via the Internet at <http://pubs.acs.org>.

References

- (1) Martin, W. R.; Eades, C. E.; Thompson, J. A.; Huppler, R. E.; Gilbert, P. E. The effects of morphine- and nalorphine-like drugs in the nondependent and morphine-dependent chronic spinal dog. *J. Pharmacol. Exp. Ther.* **1976**, *197*, 517–532.
- (2) Bowen, W. D. Sigma receptors: recent advances and new clinical potentials. *Pharm. Acta Helv.* **2000**, *74*, 211–218.
- (3) Hellewell, S. B.; Bowen, W. D. A sigma-like binding site in rat pheochromocytoma (PC12) cells: decreased affinity for (+)-benzomorphans and lower molecular weight suggest a different sigma receptor form from that of guinea pig brain. *Brain Res.* **1990**, *527*, 235–236.
- (4) Itzhak, Y.; Stein, I. Regulation of sigma receptors and responsiveness to guanine nucleotides following repeated exposure of rats to haloperidol: further evidence for multiple sigma binding sites. *Brain Res.* **1991**, *566*, 166–172.
- (5) Quirion, R.; Bowen, W. D.; Itzhak, Y.; Junien, J. L.; Mustacchio, J. M.; Rothman, R. B.; Su, T. P.; Tam, S. W.; Taylor, D. P. A proposal for the classification of sigma binding sites. *Trends Pharmacol. Sci.* **1992**, *13*, 85–86.

- (6) McLean, S.; Weber, E. Autoradiographic visualization of haloperidol-sensitive sigma receptors in guinea-pig brain. *Neuroscience* **1988**, *25*, 259–269.
- (7) Matsumoto, R. R.; Hemstreet, M. K.; Lai, N. L.; Thurkauf, A.; De Costa, B. R.; Rice, K. C.; Helleweel, S. B.; Bowen, W. D.; Walker, J. M. Drug specificity of pharmacological dystonia. *Pharmacol., Biochem. Behav.* **1990**, *36*, 151–155.
- (8) Wolfe, S. A., Jr.; Culp, S. G.; De Souza, E. B. Sigma-receptors in endocrine organs: identification, characterization, and autoradiographic localization on rat pituitary, adrenal, testis, and ovary. *Endocrinology* **1989**, *124*, 1160–1172.
- (9) Su, T. P.; London, E. D.; Jaffe, J. H. Steroid binding at sigma receptors suggests a link between endocrine, nervous, and immune systems. *Science* **1988**, *240*, 219–221.
- (10) Marrazzo, A.; Prezzavento, O.; Pappalardo, M. S.; Bousquet, E.; Iadanza, M.; Pike, V. W.; Ronsisvalle, G. Synthesis of (+)- and (–)-*cis*-2-((1-adamantylamino)-methyl)-1-phenylcyclopropane derivatives as high affinity probes for sigma1 and sigma2 binding sites. *Farmacologia* **2002**, *57*, 45–53.
- (11) Patrick, S. L.; Walker, J. M.; Perkel, J. M.; Lockwood, M.; Patrick, R. L. Increases in rat striatal extracellular dopamine and vacuolar sequestration produced by two sigma receptor ligands. *Eur. J. Pharmacol.* **1993**, *231*, 243–249.
- (12) Hanner, M.; Moebius, F. F.; Flandorfer, A.; Knaus, H. G.; Striessnig, J.; Kempner, E.; Glossmann, H. Purification, molecular cloning, and expression of the mammalian sigma1-binding site. *Proc. Natl. Acad. Sci. U.S.A.* **1996**, *93*, 8072–8077.
- (13) Kekuda, R.; Prasad, P. D.; Fei, J.-Y.; Leibach, F. H.; Ganapathy, V. Cloning and functional expression of the human type 1 sigma receptor (hSigmaR1). *Biochem. Biophys. Res. Commun.* **1996**, *229*, 553–558.
- (14) Wyrick, S. D.; Booth, R. C. Progress in sigma receptor research. *Drugs Future* **1995**, *20*, 1033–1044.
- (15) Debonnel, G.; de Montigny, C. Modulation of nmda and dopaminergic neurotransmissions by sigma ligands: possible implications for the treatment of psychiatric disorders. *Life Sci.* **1996**, *58*, 721–734.
- (16) Monnet, F. P.; Debonnel, G.; de Montigny, C. In vivo electrophysiological evidence for a selective modulation of N-methyl-D-aspartate-induced neuronal activation in rat CA3 dorsal hippocampus by sigma ligands. *J. Pharmacol. Exp. Ther.* **1992**, *261*, 123–130.
- (17) Maurice, T.; Lockhart, B. P. Neuroprotective and anti-amnesic potentials of sigma (σ) receptor ligands. *Prog. Neuro-Psychopharmacol. Biol. Psychiatry* **1997**, *21*, 69–102.
- (18) King, M.; Pan, X. Y.; Mei, J.; Chang, A.; Xu, J.; Pasternak, G. W. Enhanced κ -opioid receptor-mediated analgesia by antisense targeting the σ_1 receptor. *Eur. J. Pharmacol.* **1997**, *331*, R5–R6.
- (19) McCracken, K. A.; Bowen, W. D.; Walker, F. O.; de Costa, B.; Matsumoto, R. R. Two novel σ receptor ligands, BD1047 and LR172, attenuate cocaine-induced toxicity and locomotor activity. *Eur. J. Pharmacol.* **1999**, *370*, 225–232.
- (20) Modell, S.; Naber, D.; Holzbach, R. Efficacy and safety of an opiate sigma-receptor antagonist (SL 82.0715) in schizophrenic patients with negative symptoms: an open dose-range study. *Pharmacopsychiatry* **1996**, *29*, 63.
- (21) Huber, M. T.; Gotthardt, U.; Schreiber, W.; Krieg, J. C. Efficacy and safety of the sigma receptor ligand EMD 57445 (panamesine) in patients with schizophrenia: an open clinical trial. *Pharmacopsychiatry* **1999**, *32*, 68–72.
- (22) Walker, J. M.; Bowen, W. D.; Walker, F. O.; Matsumoto, R. R.; de Costa, B.; Rice, K. C. Sigma receptors: biology and function. *Pharmacol. Rev.* **1990**, *42*, 355–402.
- (23) Hellewell, S. B.; Bruce, A.; Feinstein, G.; Orringer, J.; Williams, W.; Bowen, W. D. Rat liver and kidney contain high densities of sigma 1 and sigma 2 receptors: characterization by ligand binding and photoaffinity labeling. *Eur. J. Pharmacol.* **1994**, *268*, 9–18.
- (24) Bastianetto, S.; Perrault, G.; Sanger, D. J. Pharmacological evidence for the involvement of sigma sites in DTG-induced contralateral circling in rats. *Neuropharmacology* **1995**, *34*, 107–114.
- (25) Jeanjean, A. P.; Laterre, E. C.; Maloteaux, J. M. Neuroleptic binding to sigma receptors: possible involvement in neuroleptic-induced acute dystonia. *Biol. Psychiatry* **1997**, *41*, 1010–1019.
- (26) Vilner, B. J.; John, C. S.; Bowen, W. D. Sigma-1 and sigma-2 receptors are expressed in a wide variety of human and rodent tumor cell lines. *Cancer Res.* **1995**, *55*, 408–413.
- (27) Crawford, K. W.; Bowen, W. D. Sigma-2 receptor agonists activate a novel apoptotic pathway and potentiate antineoplastic drugs in breast tumor cell lines. *Cancer Res.* **2002**, *62*, 313–322.
- (28) Vilner, B. J.; Bowen, W. D. Modulation of cellular calcium by sigma-2 receptors: release from intracellular stores in human SK-N-SH neuroblastoma cells. *Pharmacol. Exp. Ther.* **2000**, *292*, 900–911.
- (29) Crawford, K. W.; Coop, A.; Bowen, W. D. σ_2 receptors regulate changes in sphingolipid levels in breast tumor cells. *Eur. J. Pharmacol.* **2002**, *443*, 207–209.
- (30) Caveliers, V.; Everaert, H.; Lahoutte, T.; Dierickx, L. O.; John, C. S.; Bossuyt, A. Labelled sigma receptor ligands: can their role in neurology and oncology be extended? *Eur. J. Nucl. Med. Mol. Imaging* **2001**, *28*, 133–135.
- (31) Friebe, M.; Mahmood, A.; Bolzati, C.; Drews, A.; Johannsen, B.; Eisenhut, M.; Kraemer, D.; Davison, A.; Jones, A. G. 99mTc oxotechnetium(V) complexes amine–amide–dithiol chelates with dialkylaminoalkyl substituents as potential diagnostic probes for malignant melanoma. *J. Med. Chem.* **2001**, *44*, 3132–3140.
- (32) Choi, S. R.; Yang, B.; Plossl, K.; Chumpradit, S.; Wey, S. P.; Acton, P. D.; Wheeler, K. T.; Mach, R. H.; Kung, H. F. Development of a Tc-99m labeled sigma-2 receptor-specific ligand as a potential breast tumor imaging agent. *Nucl. Med. Biol.* **2001**, *28*, 657–666.
- (33) Zampieri, D.; Mamolo, M. G.; Laurini, E.; Zanette, C.; Florio, C.; Collina, S.; Urbano, M.; Azzolina, O.; Vio, L. Substituted benzo-(d)oxazol-2(3H)-one derivatives with preference for the sigma1 binding site. *Eur. J. Med. Chem.* **2009**, *44*, 124–30.
- (34) Glennon, R. A.; Ablordepey, S. Y.; Ismaiel, A. M.; El-Ashmawy, M. B.; Fischer, J. B.; Howie, K. B. Structural features important for sigma1 receptor binding. *J. Med. Chem.* **1994**, *37*, 1214–19.
- (35) Ablordepey, S. Y.; Fischer, J. B.; Law, H.; Glennon, R. A. Probing the proposed phenyl-A region of the sigma-1 receptor. *Bioorg. Med. Chem.* **2002**, *10*, 2759–2765.
- (36) Glennon, R. A. Pharmacophore identification for sigma-1 (σ_1) receptor binding: application of the “deconstruction–reconstruction–elaboration” approach. *Mini-Rev. Med. Chem.* **2005**, *5*, 927–940.
- (37) Gund, T. M.; Floyd, J.; Jung, D. Molecular modeling of σ_1 receptor ligands: a model of binding conformational and electrostatic considerations. *J. Mol. Graphics Modell.* **2004**, *22*, 221–230.
- (38) *Catalyst*, version 4.9; Accelrys Inc.: San Diego, CA.
- (39) Wang, H.; Duffy, R. A.; Boykow, G. C.; Chackalamannil, S.; Madison, V. S. Identification of novel cannabinoid CB1 receptor antagonist by using virtual screening with a pharmacophore model. *J. Med. Chem.* **2008**, *51*, 2493–2446.
- (40) Guner, O.; Clement, O.; Kurogi, Y. Pharmacophore modeling and three-dimensional data bases searching for drug desing using Catalyst: recent advances. *Curr. Med. Chem.* **2004**, *11*, 2991–3005.
- (41) Sutter, J.; Guner, O. F.; Hoffman, R. D.; Li, H.; Wadman, M. Effect of Variable Weight and Tolerances on Predictive Model Generation. In *Pharmacophore Perception, Development, and Use in Drug Design*; Guner, O. F., Ed.; International University Line: La Jolla, CA, 1999; pp 501–511.
- (42) Laggner, C.; Schieferer, C.; Fiechtner, B.; Poles, G.; Hoffmann, R. D.; Glossmann, H.; Langer, T.; Moebius, F. Discovery of high-affinity ligands of σ_1 receptor, ERG2, and emopamil binding protein by pharmacophore modeling and virtual screening. *J. Med. Chem.* **2005**, *48*, 4754–4764.
- (43) Sam, J.; Valentine, J. L.; Aboul-Enein, M. N. Reaction of 3-(choroalkyl)-2-benzoxazolinones with amines. Formation of 3-(aminoalkyl)-2-benzoxazolinones and 5-substituted 2,3,4,5-tetrahydro-1,5-benzoxazepines. *J. Pharm. Sci.* **1971**, *60*, 1370–1375.
- (44) Mokrosz, M. J.; Kowalski, P.; Kowalska, T.; Majka, Z.; Duszynska, B.; Bojarski, A. J.; Fruzinski, A.; Karolak-Wojciechowska, J.; Wesolowska, A.; Klodzinska, A.; Tatarczynska, E.; Chojnacka-Wojcik, E. Structure–activity relationship studies of CNS agents. Part 38. Novel 1,4-benzoxazin-3(4H)-one, 1,2-benzoxazolin-3-one and 1,3-benzoxazolin-2,4-dione arylpiperazine derivatives with different 5-HT_{1A} and antagonistic 5-HT_{2A} activities. *Arch. Pharm.* **1999**, *332*, 373–379.
- (45) Freund, R.; Mederski, W. W. K. R. A convenient synthetic route to spiro(indole-3,4'-piperidin)-2-ones. *Helv. Chim. Acta* **2000**, *83*, 1247–1255.
- (46) Lunn, G.; Sansone, E. B. Facile reduction of pyridines with nickel–aluminum alloy. *J. Org. Chem.* **1986**, *51*, 513–517.
- (47) Alabaster, V. A.; Campbell, S. F.; Danilewicz, J. C.; Greengrass, C. W.; Plews, R. M. 2,4-Diamino-6,7-dimethoxyquinazolines. 2. 2-(4-Carbamoylpiperidino) derivatives as alpha 1-adrenoceptor antagonists and antihypertensive agents. *J. Med. Chem.* **1987**, *30*, 999–1003.
- (48) Atrash, B.; Bradley, M.; Kobylecki, R.; Cowell, D.; Reader, J. Revolutionizing resin handling for combinatorial synthesis. *Angew. Chem., Int. Ed.* **2001**, *40*, 938–941.

- (49) Mamolo, M. G.; Zampieri, D.; Zanette, C.; Florio, C.; Collina, S.; Urbano, M.; Azzolina, O.; Vio, L. Substituted benzylaminoalkylindoles with preference for the σ_2 binding site. *Eur. J. Med. Chem.* **2008**, *43*, 2073–2081.
- (50) Brooks, B. R.; Brucoleri, R. E.; Olafson, B. D.; States, D. J.; Swaminathan, S.; Karplus, M. J. CHARMM: a program for macromolecular energy, minimization, and dynamics calculations. *J. Comput. Chem.* **1983**, *4*, 187–217.
- (51) Smellie, A.; Teig, S. L.; Towbin, P. Poling: promoting conformational variation. *J. Comput. Chem.* **1994**, *16*, 171–187.
- (52) Smellie, A.; Kahn, S. D.; Teig, S. L. Analysis of conformational coverage. 1. Validation and estimation of coverage. *J. Chem. Inf. Comput. Sci.* **1995**, *35*, 285–294.
- (53) Smellie, A.; Kahn, S. D.; Teig, S. L. Analysis of conformational coverage. 2. Applications of conformational models. *J. Chem. Inf. Comput. Sci.* **1995**, *35*, 295–304.
- (54) Langer, T.; Krovat, E. M. Chemical-feature based pharmacophores and virtual library screening for discovery of new leads. *Curr. Opin. Drug Discovery Dev.* **2003**, *6*, 370–376.
- (55) Fisher, R. *The Design of Experiments*; Hafner Publishing: New York, 1966.